ALGORITHM DEFINITION FOR THE VLSI DESIGN IMPLEMENTATION OF THE ELECTROMAGNETIC RADIATION INTEGRAL

THESIS

Lawrence E. Jones Captain, USAF

AFIT/GE/ENG/85D-23

DEPARTMENT OF THE AIR FORCE
AIR UNIVERSITY
AIR FORCE INSTITUTE OF TECHNOLOGY

Wright-Patterson Air Force Base, Ohio

(1)

AFIT/GE/ENG/85D-23

ALGORITHM DEFINITION FOR THE VLSI

DESIGN IMPLEMENTATION OF THE

ELECTROMAGNETIC RADIATION INTEGRAL

THESIS

Lawrence E. Jones Captain, USAF

AFIT/GE/ENG/85D-23

AFIT/GE/ENG/85D-23

ALGORITHM DEFINITION FOR THE VLSI DESIGN IMPLEMENTATION OF THE ELECTROMAGNETIC RADIATION INTEGRAL

THESIS

Presented to the Faculty of the School of Engineering

of the Air Force Institute of Technology

Air University

In Partial Fulfillment of the

Requirements for the Degree of

Master of Science in Electrical Engineering

Lawrence E. Jones, B.S.

Captain, USAF

December 1985

Approved for public release; distribution unlimited

Preface

Initially, I thought the brunt of my effort on this study would involve the architecture definition of a set of silicon chips that would digitally calculate the vector potential (A), output out of the radiation integral. It was my understanding that this radiation integral has been known of for many moons, so surely locating the algorithm needed for digital implementation should have been a relatively straightforward process. I was told it was being done in software, and that was really the basis for undertaking the project, to cut down on the software overhead time. It was a perfect study topic choice for me, applying state-of-the-art digital techniques to a classic problem.

All the solutions I thought I would draw my algorithm from use a far-field approximation that deals with at most only two-dimensional problems. I was after a more general animal that provided three-dimensional solutions in both the near- and far-field regions. A rather simple numerical summation integration scheme proved to be the best solution method that adequately deals with the general vector potential problem. Unfortunately, the vector potential is only an intermediate value that is used in the mathematical process of finding the electric (E) and magnetic (H) fields generated from a radiating antenna. Quirks that arise from numerical techniques, dictate that it is not a wise decision to try and derive E and H from the vector potential numerically. This defines the path that follow on work should take. The numerical algorithm should solve for E and H, not A.

Although the numerical algorithm definition stage ate up most of the research time, I did get to spend some time looking into the digital algorithms that perform the required mathematical operations. I found it rather fascinating to see how say, division is turned into a multiplication and addition process. I think the difficulty that will be experienced in this area during follow on work, will be in intelligently choosing which algorithm to use, given the vast variety that exist for each mathematical operation.

I'd like to thank various members of the staff here at AFIT, for it is these people that are the key ingredients that allowed me to achieve any success at all. Dr. Terzouli dreamt the initial idea up, and worked with me throughout the whole period. Dr. Pyati informed me of Filon's method and 1Lt. Jost helped me with dipole analysis and suggested I talk to Dr. Lee. Lt. Colonel Carter was consulted early in the process and selected additional classes I would need to adequately deal with the digital aspect of the problem. Captain Prescott taught one of those classes and helped me discard the FFT solution method. Captain Linderman (computer architecture) became interested enough in the topic to sign on as a committee member. His expertise in the digital area was counted on

heavily with regards to digital implementation. Dr. Jones located the text that showed me how to do the three-dimensional expansions. Captain Clemens worked with me on the three-to two-dimensional transformation. Dr. Quinn pointed out significant points about the digital algorithms. I'd like to submit a special thanks to Dr. David Lee, head of the AFIT Math and Computer Science department. Although incredibly busy with other matters, he spent an extraordinary amount of time helping me work to a conclusion. Without his incomplete cylindrical functions (ICF) closed form solution, I would have had no means with which to check the validity of my algorithm.

Finally, I'd like to acknowledge that the team effort to produce this study not only included the academic arena, but also my entire family. My children (Phillip and Rachel), may not know what a vector potential is, but they sure are familiar with "not now, I'm working on my thesis". My wife Debra got to suffer through all the cussing and hair pulling right along with me, she even got to type it up. I've found the effort to be an enlightening experience. Thanks to all those that helped me through it.

Table of Contents

Page

List of Figures

List of Tables

Abstract

A classic method used to solve for the electric (E) and magnetic (H) fields produced by a radiating source involves first solving for the vector potential (A) through the evaluation of the radiation integral. This study was undertaken to define a numerical algorithm that solves for A, so that a reduction in computation time can be realized through VLSI design implementation.

Fast Fourier Transforms, Newton-Cotes numerical integration, and variable parameterization, were applied to the problem with unsuccessful results. A numerical summation approximation proved to have all the desired qualities for the algorithm. These qualities are, ability to handle arbitrary antennas, accurate results, and all digital mathematics algorithms exist. Verification of the numerical solution was accomplished by comparing the results it produced for a dipole antenna with a triangular shaped current density against the far-field approximation, and an incomplete cylindrical functions solution developed by Lee.

Solution for E and H involves taking derivatives of A. Complications that arise from numerical techniques dictate that numerical differentiation should be performed before numerical integration. Follow on work on this topic will therefore have to focus on this detail before the actual VLSI chip architecture definition stage can be addressed.

ALGORITHM DEFINITION FOR THE VLSI DESIGN IMPLEMENTATION OF THE ELECTROMAGNETIC RADIATION INTEGRAL

Chapter I

Problem Definition / Solution / Results Overview

Statement of The Problem

In 1864 James Clerk Maxwell read his paper "A Dynamical Theory of the Electromagnetic Field" to the royal society (1:282). The theories he brought together and formulated into the now famous "Maxwell Equations", have been the building blocks for today's electronic age. The common practice method of utilizing Maxwell's Equations to determine the pattern produced by a radiating source (antenna), involves first solving for a quantity known as the vector potential (A) (2:82-87) (3:9-13) through the evaluation of the radiation integral. The desired E (electric) and H (magnetic) fields are obtained from the vector potential by employing the following two equations.

$$H = \nabla \times A \tag{1}$$

$$E = \frac{1}{j\omega\epsilon} \nabla \times H \tag{2}$$

Equation (3) and Figure 1 define the mathematical expression and geometry used for the vector potential.

$$A(\bar{r}) = \iiint_{V\bar{r}'} \frac{J(\bar{r}')\, e^{-jk|\bar{r}-\bar{r}'|}}{4\pi\, |\bar{r}-\bar{r}'|}\, d\bar{r}' \qquad (3)$$

k = wave number = $2\pi/\lambda$

$J(\bar{r}')$ = current density on the antenna

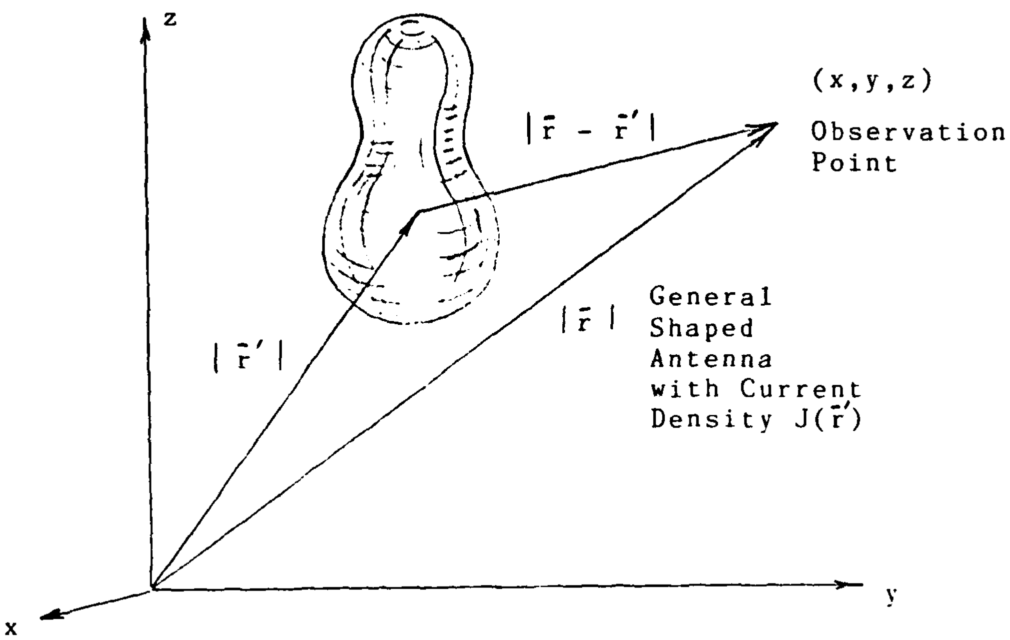

Figure 1

Arbitrary antenna and observation point

Although the solution of Maxwell's Equations to this point is conceptually very clear, progress past this integral is quite painful. Analysis of even the simplest antennas and current densities requires the solution of a complex integral. Early solutions of the problem employed the use of a far-field approximation (3:25). This approximation simplified the integration process enough so that it could be done, but left the person wanting to know what the field was like near the antenna, empty-handed. Many great minds have spent a great deal of time trying to develop the mathematical tools needed to deal with this problem. The advent of the computer in the electronic age, is probably the big breakthrough which will ultimately reduce the problem down to doable terms.

The 1960's saw people applying this new tool, the computer, to the numerical solution of the radiation integral (4:54-61). Even with this tremendous increase in calculating power, the radiation integral proves to be more than a match for multi-user time-sharing computer systems. It just isn't practical to think we have reduced the problem down to its simplest form, when it takes a day to solve for the pattern at one point in space.

This study was undertaken to assess the feasibility of developing a set of dedicated silicon chips that evaluates the radiation integral (both near- and far-field) in a reasonable time period (< minutes) for any general shaped antenna. The basic concept is that an operation like addition takes μ seconds when performed by software in a computer. The same operation takes nano-seconds in a silicon chip. A reduction of three orders of magnitude in calculation time would be a significant step towards finding the solution in an acceptable time.

The second big reduction in processing time can be achieved by using pipelined parallel processors. As shown in (3:11), solution of Maxwell's Equation for the vector potential is broken up into evaluating three scalar equations. Three parallel processors can work on the problem at the same time, unlike the software solution that must evaluate each equation one at a time. Pipelining is nothing more than an efficient use of the processor's time. The system is set-up such that the main processor's wait time for input data is kept to a minimum.

Solution Attempt Overview

Use of Fast Fourier Transform (FFT) techniques was the first approach tried in the attempt to embed the radiation integral into silicon. Work along these lines was not pursued to any great extent after a preliminary look at the situation showed that the radiation integral's spatial dependence complicated the process tremendously. See Chapter II for details.

A numerical integration scheme such as Simpson's Rule or Gaussian Quadrature was next given a try. After some fairly extensive work in the numerical integration arena, a modified Simpson's Rule known as Filon's Method was chosen as the one to use.

Newton-Cotes integration schemes like Filon's, depend on having a continuous function over the interval of integration. Examination of Figure 1 and Equation (3) shows that the integration of a general antenna is over a three-dimensional surface current. The surface current is not continuous in the three dimensions thereby eliminating these numerical integration techniques.

Two options remained. Mathematically the three-dimensional surface currents can be mapped onto a two-dimensional plane (aperture) and then a continuous two-dimensional numerical integration scheme can be carried out. This mapping process turns the limits of integration into functions of the variables, which makes digital implementation of any generalized antenna impossible. The second alternative ended up being the proposed algorithm. It is discussed in the next section.

Although numerical integration did not yield the solution to the radiation integral problem, some worthwhile work was accomplished in this area. Both Simpson's and Filon's integration equations were expanded out into three dimensions. See Chapter II and Appendix A for details.

Proposed Integration Algorithm

It was only after letting each of the so-called "smart" methods have their chance, and failing at solving the problem, that probably the simplest and crudest method was given a chance. The basic problem here was finding the value of a very difficult integral. Integration is nothing more than an infinite number of sums of the integrand. Equation (4) shows how the radiation integral was approximated with a finite number of summations.

The integration of the surface area is approximated by adding up a finite number of sub-area elements ΔA_j.

$$\iiint_{\gamma \bar{r}'} \frac{J(\bar{r}')e^{-jk|\bar{r}-\bar{r}'|}}{4\pi|\bar{r}-\bar{r}'|}\,d\bar{r}' \approx \sum_{j=1}^{M} \frac{\Delta A_j J_j(\bar{r}')e^{-jk|\bar{r}-\bar{r}_j'|}}{4\pi|\bar{r}-\bar{r}_j'|} \quad (4)$$

ΔA_j = Surface area of j^{th} element

$J_j(\bar{r}')$ = Current on j^{th} surface element

$\bar{r}_j'$ = Distance from origin to j^{th} surface element

The key to the success or failure of a scheme such as this, is how small does ΔA_j have to be (i.e. how large does M have to be) in order for the summation to yield accurate results. This simple approach to the problem was given its chance at solving the radiation integral because the other attempts had failed, and it had the very desirable characteristic that all the necessary algorithms needed for digital implementation exist.

The summation approximation had made it to a point where the other methods had failed to get, comparison with a given antenna and known current distribution. A simple dipole antenna with a triangular shaped current distribution was chosen as the initial test case. It was a relatively simple task to compare the summation with the far-field approximation for this antenna. Considerable effort was expended in locating an accurate closed form comparison solution of the test case antenna in the near-field region. The closed form solution proved to be unique enough to produce a journal communication to inform others of its existence (5). The solution utilizes special functions known as incomplete cylindrical functions (ICF) to solve the integral for the test antenna. See Appendix D for details on the ICF analysis. Chapter III details the summation comparison with the far-field and ICF solutions.

Summary of Results, Conclusions and Recommendations

The three solutions (far-field, ICF, summation) of the test case antenna were coded up using Fortran 77 and the results were compared for observation points in the near-field, close to far-field boundary, and far-field regions. A value for M, determined from the ball park estimate that each sub-section of the antenna had to be smaller than Ø.1   was calculated. The comparisons were conducted for values of M less than the estimate, equalling the estimate, and greater than the estimate.

The pleasing results of the check of the summation are as follows. First, realistic frequencies and antenna sizes yield reasonable values of M for the ballpark estimate. Second, comparison of the summation solution with the other two, shows at least a two-digit match in the solutions for M equalling the estimate. Higher values of M yield even more matching digits. This may not sound too impressive until you realize that the magnitude of the vector potential varies by two orders of magnitude for a range of observation points at a constant radius $\bar{r}$ from the antenna. Put into other words, one can not detect the error in the summation solution when it is graphed along with the more accurate ICF solution, in both the near-and far-field regions, for reasonable values of M ($M > 200$). See graphs in Chapter V. The numerical summation algorithm proved to be the answer to the digital implementation of the radiation integral. It produces accurate results in a reasonable time period, and it can be implemented into silicon.

There are, of course, a few more details that must be addressed, before any very large scale integrated circuit (VLSI) design is initiated. First, solving for the vector potential with the radiation integral assumes that the current densities on the antenna are known, can be calculated, or measured. This may require extensive numerical techniques for some complex antenna shapes. Second, as stated at the beginning of this chapter, the desired E and H fields are calculated from the vector potential through derivatives. Work in the late stages of this study discovered that numerical differentiation after numerical integration, is not a wise idea. One has to be very careful about choosing the integral length for the numerical differentiation in relationship to the segment size used in the numerical integration. To eliminate this problem, the next efforts that deal with this topic should be spent examining what needs to be done to bring the cross products inside the integral so that the summation approximation is actually solving for the E and H fields.

Although this study did not actually develop a radiation integral silicon chip, it has supplied the valuable ground work needed to show that a summation approximation of this integral yields valid results. The stage is now set to complete the task.

Chapter II

Nonusuable Solution Methods

Introduction

Fast Fourier Transform (FFT) techniques, and Newton-Cotes numerical integration schemes, were the first methods tested in the search for the solution to the integration problem. Solution from a more mathematical approach, variable parameterization, was also considered and discarded. Difficulties were encountered in trying to apply these first three preliminary methods even before they got to the stage of comparison with a given antenna and known current distribution.

Analysis through FFT's was not discounted as unusable, but rather abandoned in the hopes of finding an easier solution. The Newton-Cotes integration schemes were found to be unusable. It was only after some rather extensive work, that this fact was verified. This chapter explains what was tried, and why it failed. Appendix A contains the full three-dimensional expansion of Simpson's rule and a partial list of Filon's method expansion. The chapter concludes with an explanation of why a more pure mathematical approach also fell short in dealing with the given problem.

Fast Fourier Transform (FFT) Solution Attempt

From (2:85) or (3:11) the time harmonic nonhomogeneous scalar wave equation for the vector potential has the following form.

$$\nabla^2 A_i(\bar{r}) + k^2 A_i(\bar{r}) = -J_i(\bar{r}') \tag{5}$$

(i = x, y, or z)

or rewritten

$$A_i(\bar{r})\left[\nabla^2 + k^2\right] = -J_i(\bar{r}') \tag{6}$$

The well known solution to this equation (2:91) is:

$$A_i(\bar{r}) = \int_{\forall \bar{r}'} J_i(\bar{r}')\,\psi(\bar{r}-\bar{r}')\,d\bar{r}' \tag{7}$$

where:

$$\psi = \frac{e^{-jk|\bar{r}-\bar{r}'|}}{4\pi|\bar{r}-\bar{r}'|} \tag{8}$$

An almost immediate response from anyone familiar with circuit theory, would be to say that Equation (7) looks just like a convolution integral (6:222) :

$$Y(t) = \int_{-\infty}^{\infty} X(\tau)\,h(t-\tau)\,d\tau \tag{9}$$

where h(t) is the system transfer function

If in fact Equation (7) is a convolution integral, then $A_i(\bar{r})$ can be solved for through the following equation:

$$A_i(\bar{r}) = \mathcal{F}^{-1}\left[J_i(k)\,\psi(k) \right] \tag{10}$$

Where $\mathcal{F}^{-1}$ stands for the inverse Fourier transform.

$J_i(k)$ & $\psi(k)$ are Fourier transforms of:

$J_i(\bar{r}')$ & $\psi(\bar{r})$

It was known that functions $J_i(\bar{r}')$ and $\psi(\bar{r})$ would not be continuous functions, but rather discrete values derived from a method of moments program or measurement etc. For this reason, the discrete Fourier transform (DFT) would have to be used in Equation (10), not the continuous form. For those not familiar with FFT's, they are merely efficient time saving DFT's.

Research was initiated in the DFT/FFT area, with the following results. From (9:100) the basic form of the DFT is:

$$X(k) = \begin{cases} \sum_{n=0}^{N-1} x(n)\, W_N^{kn}, & 0 \le k \le N-1 \\ 0 & \text{ELSEWHERE} \end{cases} \tag{11}$$

$$\left(W_N^{kn} = e^{-j2\pi kn/N} \right)$$

$(\bar{r})$ has the possibility of being three-dimensional, so the DFT of $\psi(\bar{r})$ would look something like this:

$$\psi(k,l,q) = \sum_{n=0}^{N-1} \sum_{m=0}^{M-1} \sum_{p=0}^{P-1} \frac{e^{-jK|X^2+Y^2+Z^2|^{1/2}}}{4\pi |X^2+Y^2+Z^2|^{1/2}} \times e^{-j(\frac{2\pi}{N})kn} e^{-j(\frac{2\pi}{M})lm} e^{-j(\frac{2\pi}{P})qp} \qquad (12)$$

This equation made one sit back, ponder awhile, and ask is this really the direction to take to solve the radiation integral problem? It was during consultation with the study committee members (8;9) on this subject of three-dimensional FFT's that another problem surfaced.

The premise for choosing this path had been the fact that Equation (7) resembled a convolution integral. Closer examination of the quantity $(\bar{r} - \bar{r}')$ in (7) reveals that it is a representation for the vector $|\bar{r} - \bar{r}'|$, not the rotate and shift that it represents in a convolution integral. Equation (7) is not a convolution integral therefore, and even if it could be mathematically manipulated into one, the complexity of Equation (12) makes one wonder if the time would be well spent. Solution through the use of FFT's was abandoned at this point, in hopes of finding a more straightforward approach to the solution. They were not dismissed as totally unusable, but rather left to sit in the background while other methods were given their chance.

Newton-Cotes Integration Schemes

The application of a well defined numerical integration scheme seemed to be a logical step towards solving the radiation integral. Indeed, numerous comparisons of different integration schemes applied to the one- and two-dimensional radiation integral can be reviewed in the literature (10;11;12;13) as examples. The superiority of Romberg's method (11) or a piecewise linear rule (12) etc. have been documented for some time.

One- and two-dimensional antennas, however, are a somewhat special breed, in that they are either line or aperture antennas. Examination of Figure 1 shows that the general antenna dealt with in this study is really a three-dimensional surface antenna. This does not fit into either the line or aperture antenna category. The analysis, or algorithm definition of the general three-dimensional surface antenna was therefore still open for exploration.

After some research into the field of numerical integration, it was decided that Simpson's rule was the best choice, of the various schemes available, to have the first crack at solving the problem. All the literature showed how the simpler trapezoidal rule scheme was less accurate than Simpson's rule. This stems from the fact that the intervals the integral is broken up into are linked together with parabolas for Simpson's rule, as opposed with straight lines in the trapezoidal rule. The parabolas more closely approximate the actual function between the intervals. A scheme like Gaussian quadrature has desirable characteristics in that it takes fewer repetitions to arrive at the answer, but the price to pay for this reduction in computations is a significantly more difficult integration scheme. This more complex integration method is not readily applicable to the general shaped antenna.

Having decided on Simpson's rule, Equation (13), at least as the starting point, the next step was to expand it out into three-dimensions.

$$\int_a^b f(x)\,dx \approx \frac{h}{3}\left[f(a) + 2\sum_{j=1}^{M-1} f(x_{2j}) + 4\sum_{j=1}^{M} f(x_{2j-1}) + f(b) \right] \tag{13}$$

Burdon, et al. (14:172-173) showed how to perform the expansion out into two-dimensions. The three-dimensional expansion begins like this:

$$\int_a^b \int_c^d \int_e^f f(x,y,z)\,dz\,dy\,dx ;$$

$$\int_e^f f(x,y,z)\,dz \approx \frac{h}{3}\left[f(x,y,e) + 2\sum_{j=1}^{M-1} f(x,y,z_{2j}) + 4\sum_{j=1}^{M} f(x,y,z_{2j-1}) + f(x,y,f) \right] \tag{14}$$

Each of the four terms in this expression is then expanded out in terms of y, and then x. When the dust finally settles, you are left with an expression with 64 (4x4x4) separate terms in it. (See Appendix A for the full expression).

The immediate reaction to the conclusion of this expansion is that the feasibility of such a scheme is certainly in doubt. Work was nevertheless carried on, due to another concept that was believed to be true at this point.

It has already been stated several times, that for the general antenna, the current on the antenna really just maps out a surface in three dimensions, see Figure 2. It is quite easy to see from Figure 2, that the three-dimensional integration is therefore filled with a large number of zeros. Close examination of the 64 term expansion reveals that 56 of the terms deal only with the outside corners, edge lines, and surface planes. The eight remaining terms are triple summations, that take care of the volume inside the outer box. It was believed at this stage, that if one could perform a volumetric integration filled with zeros to get a surface area, one could also carry out the integration with the constraint that the surface current of interest must fit inside the inner box. The feasibility of developing a processor to handle the eight terms was realistic.

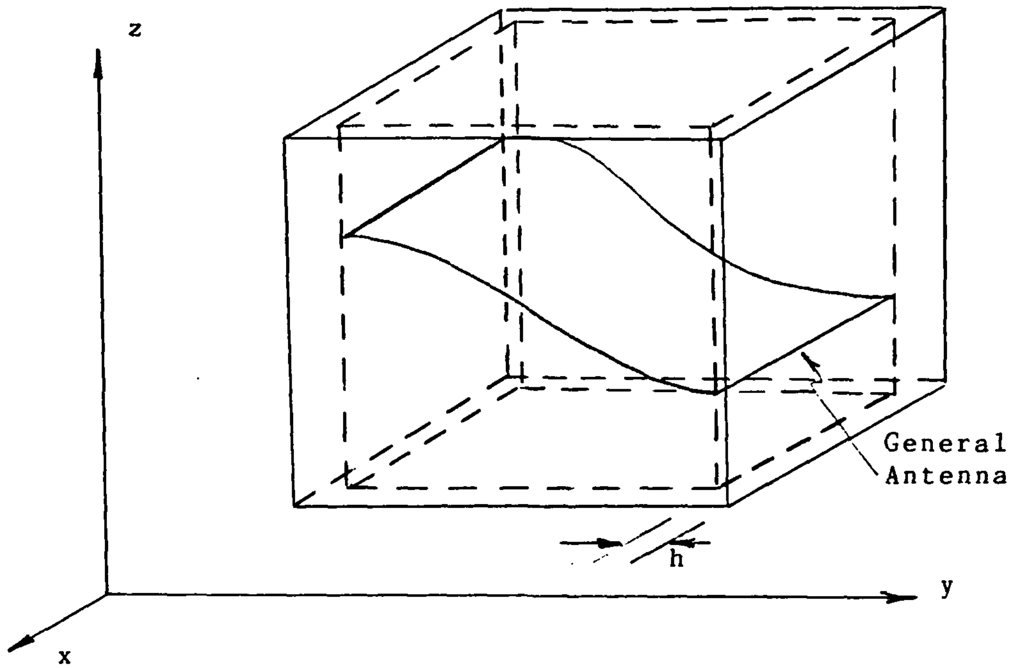

Figure 2

General antenna in three dimensions

Before work got to the point of actually trying Simpson's rule out on the radiation integral, an inherent characteristic of the integral was pointed out that eliminated this integration scheme from the running. The problem has to do with two terms in the integral, namely the current density $J(\bar{r}')$ and the exponential e^{jkr}. The exponential is really just a combination of sines and cosines (through Eulor's identity), so essentially you have a current times a sine or cosine in the integral. When realistic values are inserted for these terms, one finds that the sine and cosines have the potential of oscillating much more rapidly between the limits of integration, than the current. If accurate numerical integration is to be accomplished, extreme care must be taken when choosing the sub-interval width. It has to be small enough to adequately sample the faster oscillating sines and cosines, see Figure 3. The use of Simpson's rule was therefore ruled out due to the large number of sub-divisions the integration had to be broken up into.

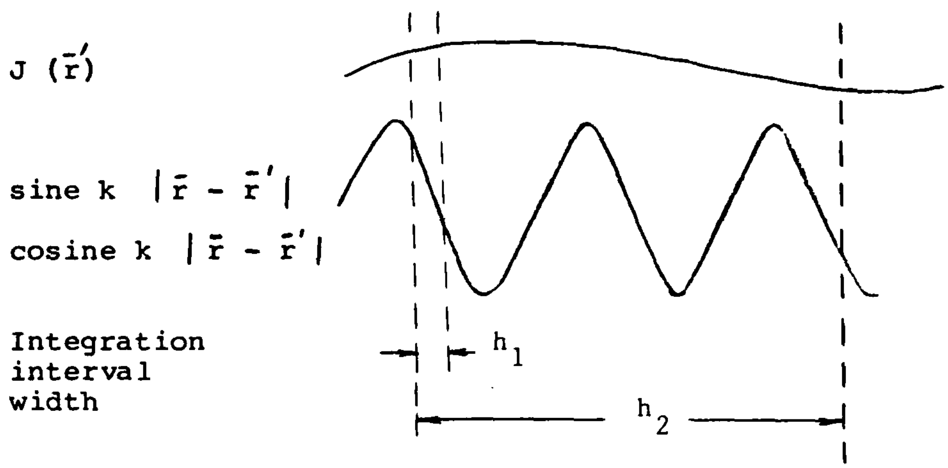

Figure 3

Slow and rapidly oscillating terms in integral

A. C. Ludwig (10) discusses this problem, and points to the solution. The problem is not new, in fact has been addressed and solved by Filon (15;16) back in 1928. Kopal (17:409) states that Filon's method is just a modification of Simpson's rule where the 2/3 & 4/3 coefficients are replaced with other coefficients and appropriate multiples of the end points are added in to compensate for this particular type of numerical integration problem. Allen (13:390) was aware of this method and, in 1959, conducted a comparison of Filon's method with other schemes for the one-dimensional case. He points out that the method works well, and talks about an expansion into two dimensions. An expansion into three-dimensions was needed for this study. This was where the experience gained in the Simpson's rule expansion was put to use.

Equation (15) shows the expression used for expansion. It is a combination of that shown in Kopal (17:408) and Burden et al. (14:172). Filon's equation takes on a slightly different form, depending on whether there are sine or cosine terms, Davis et al. (18:63) was a useful reference for the f (x) cos (mx) form.

$$\int_a^b f(x)\,\mathrm{SIN}(mx)\,dx \approx$$

$$h \Big\{ \alpha \big[f(a)\cos(ma) - f(b)\cos(mb) \big] +$$

$$\beta \Big[f(a)\,\mathrm{SIN}(ma) + f(b)\,\mathrm{SIN}(mb) + \qquad (15)$$

$$+ 2 \sum_{j=1}^{M-1} f(x_{2j})\,\mathrm{SIN}(m x_{2j}) \Big] +$$

$$\gamma \sum_{j=1}^{M} f(x_{2j-1})\,\mathrm{SIN}(m x_{2j-1}) \Big\}$$

The basic expression now has six terms, so the three-dimensional expansion has 216 terms (6x6x6) (See Appendix A). This of course is really stepping out of the feasibility realm, until you realize that 208 of these terms are once again dealing with the outside box. The analysis of the problem had progressed to the point where it was once again dealing with eight triple summations that were weighted with coefficients that had been proven to work for the one-dimensional case.

The next step, and ultimate stumbling block, was to test the idea of throwing away the outside box terms. To keep the process as simple as possible, the concept was tested out on the following integral, Equation (16), not the radiation integral.

$$\int_{-1}^{1} \cos(\pi z/2)\cos(kz)\,dz \qquad (16)$$

Figure 4a is a graphic representation of this expression. The cos ($\pi z/2$) term simulated the slowly varying current density, and the cos (kz) term was the rapidly oscillating term.

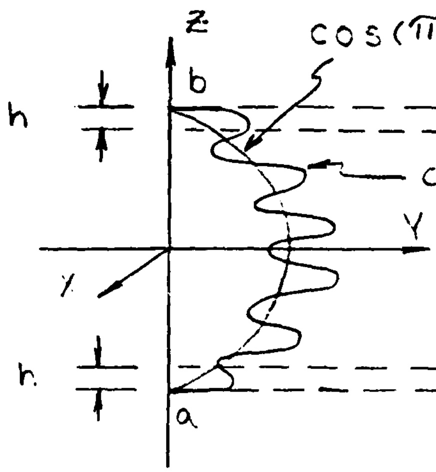

Figure 4a

Simulation with
f(a) equalling
zero at end points

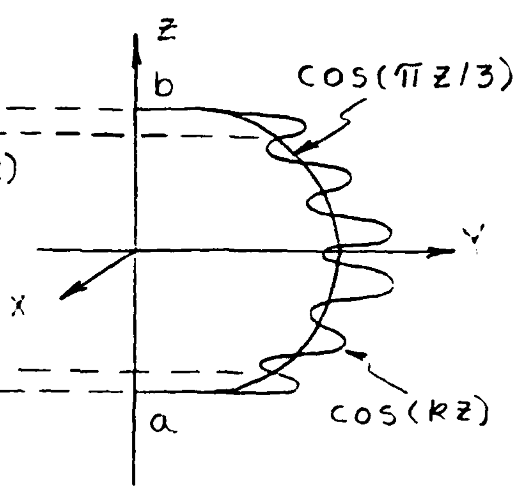

Figure 4b

Simulation with
f(a) not equalling
zero at end points

The terms of Filon's integration method that dealt with all but the endpoints were coded up using Fortran 77 and the resulting answer was compared with the closed form solution for the same interval (-1+h to 1-h). The two answers were within 3% of each other, a promising result.

It was then noted that the parts of Filon's solution that were being thrown away, the end points, were in fact equal to zero. Not much of a check to throw away zero, so another, more useful check, was devised to check the basic concept validity out. Equation (17) is the expression for the new test case pictured in Figure 4b.

$$\int_{-1}^{1} \cos(\pi z/3)\cos(kz)\,dz \qquad (17)$$

The Filon method minus the end points was once again coded up with Fortran 77 (see Appendix B), and compared with the closed form solution. The two solutions were in complete disagreement. The final straw that broke this concept's back was a comparison of results of the full Filon expression (end points included) to the closed form solution for the full interval (-1 to 1). The results agreed to within 2%. This obviously said that when you try and throw away non-zero end points, the concept falls apart. Once this point had been verified, an explanation of why the concept broke down was sought.

First of all, a basic operation of integration, established in any calculus I class, is that it finds the area under a curve. If the function between the end points fluctuates up and down, a cancellation of the positive and negative areas occurs, except at the end points. This accounts for the large error in the shortened version (without end points) of the numerical integration scheme. Ironically, it is at the two end points where all action is taking place.

Secondly, a Newton-Cotes integration scheme is based on having a continuous function between the limits of integration. Throwing away the end points, and then trying to use the formula that was developed with the end points, forces the integration method to operate on a discontinuous function, which just won't work. This simple one-dimensional test case had shown that it was going to be impossible to try and use Filon's method, or any other Newton-Cotes integration method, because the antenna current density is discontinuous in the three-dimensional volume of integration.

Mathematical Solution

So far, only the elimination of possible solution schemes had been accomplished. The Newton-Cotes integration idea had been shown to be unusable. The Fast Fourier Transform technique had been put on the back burner due to the level of complexity.

Consultation with a number of individuals (19,20,21) had taken place during the course of work up to this point. Due to the nature of the problem, most of the people solicited for advice, had been mathematicians. Each of them, after an initial introduction to the problem, suggested the same basic solution. The obvious solution, as conceived by any pure mathematician, was to simply map the three-dimensional integral onto a two-dimensional plane (aperture). See example in Figure 5. The integral equation would then take on a form similar to Equation (18).

$$A(\bar{r}) = \int_{t_1}^{t_2}\int_{t_1}^{t_2} \frac{\hat{\tau}(u_1,u_2)\, J(u_1,u_2)\, e^{-jk|\bar{r} - F(u_1,u_2)|^{1/2}}}{4\pi\,|\bar{r} - F(u_1,u_2)|^{1/2}}\, du_1\, du_2 \qquad (18)$$

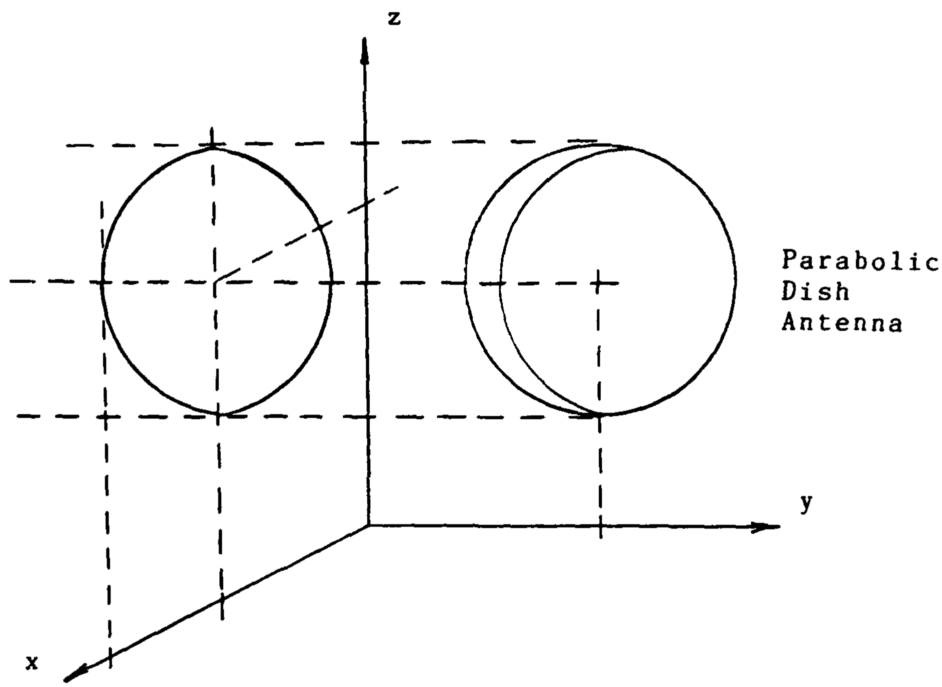

Figure 5

Mapping of three-dimensional surface to two dimensions

Equation (18) is not intended to be an entirely correct mathematical expression, but merely serve as an example expression that illustrates the following point. The limits of integration t1, t2, t3, t4, are no longer the simple constants they were for the three-dimensional cube approach, but rather functions of the new parametric variables u1 and u2. That's fine if you have a nice mathematical expression for the shape of your antenna, but one usually finds it very difficult to define that expression for any given general shaped antenna. Indeed, for realistic complex geometry antennas, it is virtually impossible to come up with the equation of the antenna. Also note the parabolic dish antenna depicted in Figure 5 maps very neatly on to a circle. Another antenna may not map into a circle, but rather an ellipse or a square or some arbitrary shape. It should be fairly clear by now, that what appears to be the obvious mathematical answer to the problem, eliminates the ability to handle general shaped antennas. This ability, was one of the many underlying goals of this study. The silicon chip processor would be very limited and of questionable use, if it could only handle say, parabolic dish antennas. For this reason, this solution concept was abandoned, and work was directed towards the fourth and final solution approach.

The reader may wonder, why this chapter exists, when quite frankly the concepts discussed and methods tried didn't solve the study problem. There are several reasons.

First, a good deal of effort was expended in expanding Simpson's rule and Filon's method into three dimensions. Although the resulting expressions (in Appendix A) could not be used for the basic radiation integral, it is felt that there is a possible use in other three-dimensional integration problems.

An even more important reason, is to document a grave conceptual error, that led a number of people down the wrong path for much too long a time. It's easy to sit back now and say, well why didn't you try throwing away the end points with Simpson's method, long before you spent all the effort on Filon's method? That question pinpoints the reason for including this chapter. That is, it is very easy while wrapped up in the furor of trying to adapt a well-established method to the details of a given problem, to neglect the basics. It is even possible to devise a check of the concept or method employed, which in itself is in error.

Finally, what may seem to be the obvious solution to some, may in fact totally change the scope of the problem. The mathematical solution did not adequately deal with the general problem.

Chapter III

Proposed Algorithm Definition

Introduction

Figure 6 shows a general shaped antenna, that has been divided up into a number of sub-area elements, ΔA_j.

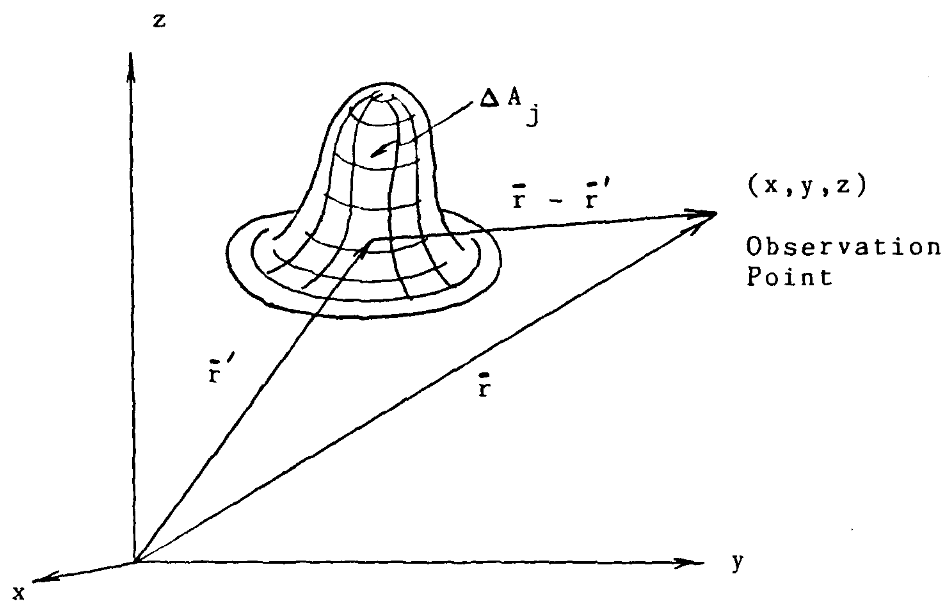

Figure 6

Sectioned general shape antenna

The numerical approximation solution to the radiation integral uses these sub-area elements as follows:

$$A(\bar{r}) = \iiint_{\forall \bar{r}'} \frac{J(\bar{r}')\, e^{-jk|\bar{r}-\bar{r}'|}}{4\pi |\bar{r}-\bar{r}'|}\, d\bar{r}' \approx \sum_{j=1}^{N} \frac{J_j(\bar{r}')\, \Delta A_j\, e^{-jk|\bar{r}-\bar{r}'_j|}}{4\pi |\bar{r}-\bar{r}'_j|} \qquad (19)$$

The concept of why the triple integral goes down to a single summation can be explained by first looking at the solution of the ideal dipole (3:14).

In the ideal dipole case, the length of the antenna, L, is much, much smaller than either the distance $|\bar{r}|$ or $|\bar{r} - \bar{r}'|$, see Figure 7.

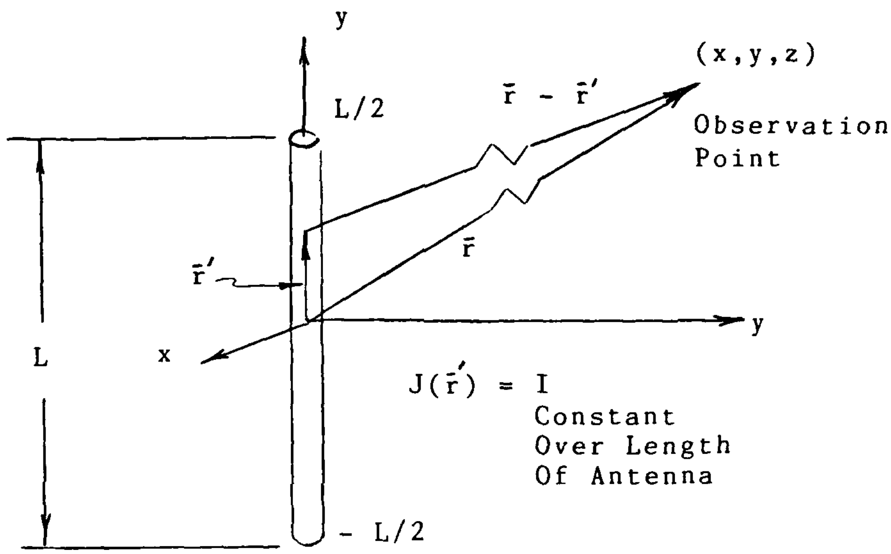

Figure 7

Ideal dipole

$|\bar{r} - \bar{r}'|$ and $|\bar{r}|$ are therefore essentially the same magnitude. This greatly simplifies the radiation integral, because all but the differential, dz', can be brought outside the integral sign.

$$A(\bar{r}) = \hat{z}\,\frac{I\,e^{-jk|\bar{r}|}}{4\pi|\bar{r}|}\int_{-L/2}^{L/2} dz' \tag{20}$$

Thus :

$$A(\bar{r}) \approx \hat{z} \frac{I e^{-jk|\bar{r}|}}{4\pi|\bar{r}|} L \qquad (21)$$

(with $|\bar{r} - \bar{r}'| \approx |\bar{r}|$)

The basic concept to be gleaned from this analysis, is that the integration process is transformed into a simple length integration.

For the antenna depicted in Figure 6, $|\bar{r} - \bar{r}'|$ is not approximately equal to $|\bar{r}|$, so the manipulation of the general integral does not follow that of the ideal dipole exactly. The concept that is borrowed from the ideal analysis, is that the integration is treated as a simple area integration for the general three-dimensional surface antenna. Of course, if the antenna is one-dimensional, the integration translates out into a length, as it did with the dipole. The area integration can then be approximated as the sum of all the sub-area elements ΔA_j (or sub-length elements Δh_j). The accuracy of the approximation is brought about by making ΔA_j, small, and associating the correct J_j and $\bar{r}'_j$ with each element.

It is quite easy to see, that this approach uses the simplest of numerical integration schemes. From Chapter II, recall that the so-called "smart" numerical integration schemes (Newton-Cotes) required a continuous function over the interval of integration. This basic numerical integration adds up the sub-elements to produce a length, area, or volume. The radiation integral represents line currents, or surface currents that reside in three dimensions. This simplistic numerical integration scheme doesn't care if the function is discontinuous in three dimensions, it simply adds up what you give it. The current and either area or length magnitude inputs can be obtained from a numerical technique like a method of moments program, or measurement.

This approach to the solution had not been given serious consideration initially due to its crudeness. It was now the front runner because it had surpassed all the hurdles where the other methods had failed. It also looked like a very promising approach in terms of implementation into a silicon chip. All the necessary algorithms needed for the transformation exist and are well studied (see Chapter IV). The time had come to see if it could proceed on, namely, how did it perform when compared with a known solution to a specified antenna?

Test Case Antenna

It appeared that the numerical solution was capable of producing the answer for the vector potential of any general shaped antenna. The big question left to be answered was, how small did ΔA_j have to be, i.e. how large did M have to be, for the summation to closely approximate the integral? A test case antenna with a known solution was required to answer this question. The one chosen is shown in Figure 8.

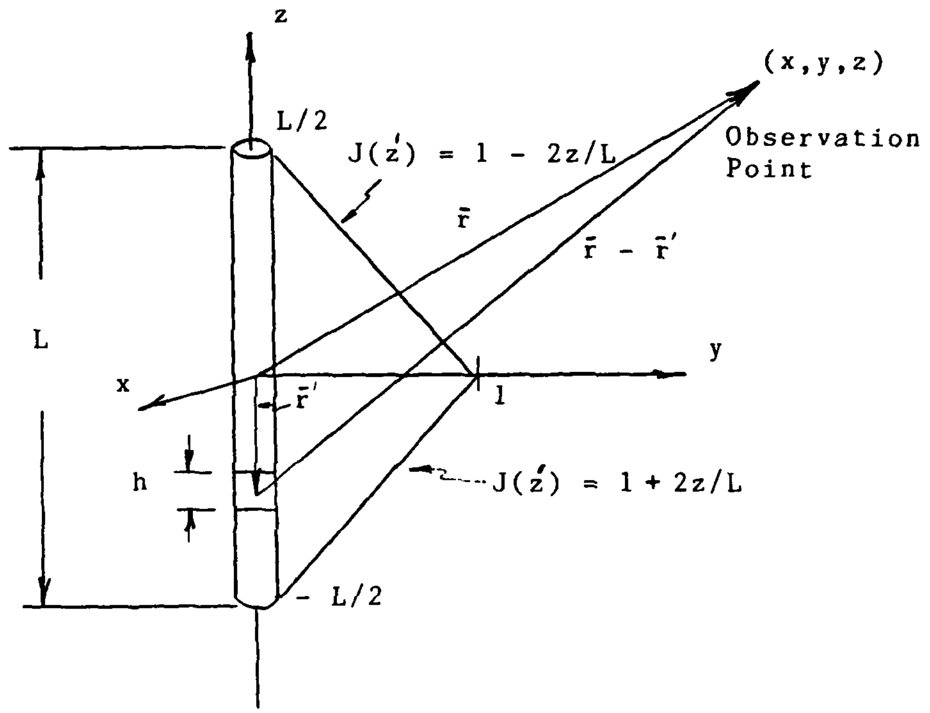

Figure 8

Test antenna and current distribution

It's the next simplest to the ideal dipole, a finite length antenna located on the z axis. The analytic triangular shaped current distribution was chosen for two reasons. One, it is a more complex distribution than a simple uniform distribution and two, the exact closed form solution was located. Location of a solution for the far-field case was of course, relatively easy, as it has been well studied and documented in almost any text on the subject. The near-field solution presented the problem. Even when it is addressed, such as in (2:285), the resulting solutions that are given, are the E (electric) and H (magnetic) fields, not the vector potential ($A(\bar{r})$). This study was interested in solving for the vector potential first, with the belief that the appropriate mathematical operations could be performed on $A(\bar{r})$ to yield E and H. The closed form solution located for the near-field comparision of the vector potential uses special functions known as incomplete cylindrical functions (ICF) (5,19,Appendix D). The expression for the vector potential is manipulated into an appropriate form and the ICF handle is cranked to yield $A(\bar{r})$. *E and H* can also be solved for by taking the appropriate derivatives of the ICF's. The literature search for the near-field solution, found no other such solution. An IEEE Transactions on Antennas and Propagation communication (5) was therefore submitted, to inform others of this particular vector potential solution.

The remainder of this chapter details the steps taken for the three solution methods. Results of the comparison of the numerical method against the far-field and ICF solutions is documented in Chapter V. The simple answer to the question, how did it do, is that it did very well for very reasonable values of M.

Numerical Solution of Test Antenna

In the manipulation of the vector potential expression into the ICF form, it was first necessary to solve for $A(\bar{r})$ with a uniform current distribution like that shown in Figure 9.

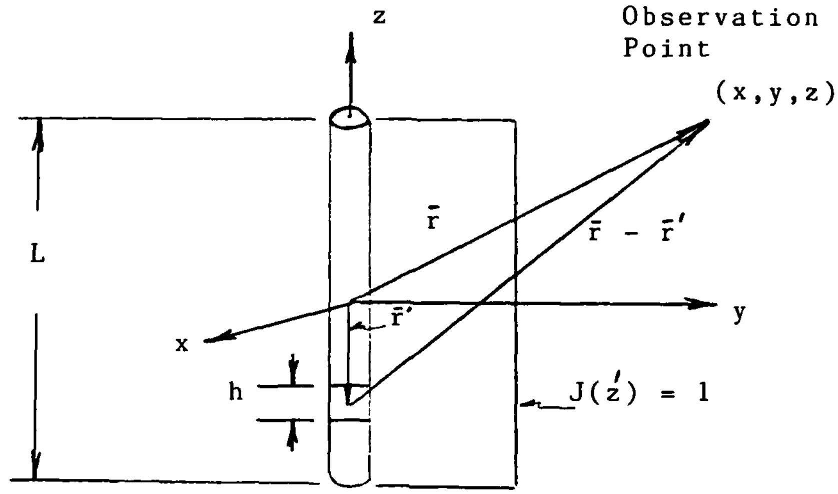

Figure 9

Uniform current distribution

For this reason the solution of the vector potential produced from both the uniform and triangular shaped current densities was solved for by each of the three methods, numerical, far-field, and ICF. This additional comparison of two current densities helped to insure that there were no hidden properties of a given current density that made the results of the test appear promising.

For the numerical solution, the dipole is first divided up into M sub-elements (See Figures 8 or 9). Each segment is assigned a uniform current distribution equalling the magnitude of the actual current density at the middle of that particular segment. This is a trivial step when the current density on the dipole is itself uniform.

The next step is to calculate the magnitude of the vector from the origin to the middle of each particular segment. This is the $\bar{r}'$ vector used to calculate $|\bar{r} - \bar{r}'|$. For the numerical solution, the vector potential takes on the following form.

$$A(\bar{r}) \approx h \sum_{j=1}^{M} \frac{J_j \, e^{-jk\left| x^2 + Y^2 + (z - \bar{z}_j')^2 \right|^{1/2}}}{4\pi \left| x^2 + Y^2 + (z - \bar{z}_j')^2 \right|^{1/2}} \tag{22}$$

h = L / M = length of sub-element

J_j = current density at center of each segment

= 1 for uniform current density

$\bar{z}_j'$ = vector to center of each segment

= -L/2 + (h x j) - (h/2)

The particular values chosen for the test are the following:

L = 1 meter

k = 63 which equates to

λ = .0997 or f = 3.008 GHZ

Simplification: Let observation point be located in the y z plane (i.e. x = 0)
This is allowable due to the inherent symmetry of the antenna with respect to the z axis.

Limitation: Make comparison in first quadrant only. Allowable once again due to antenna symmetry.

The expression was coded up in Fortran 77, and the resulting solutions for different values M were compared with the other two method's solutions. A copy of the Fortran program is included in Appendix C. The name of the program for the uniform current density is UNIFLD. The complex function routine SUMFLD, in the program was used to calculate the numerical solution. Chapter V discusses the results of the comparison.

A simple modification to the program was required to solve for $A(\bar{r})$ with the triangle shaped current density (see Figure 8). For the uniform case, J_j had a magnitude of one. J_j took on the following form for the triangle current density.

$$J_j = 1 - 2|\bar{z}'_j| / L \tag{23}$$

(where $|\bar{z}'_j|$ = absolute value of the $\bar{z}'_j$ vector)

Program TRIFLD, in Appendix C, was used to solve for the triangle shaped current density. Calculation of the above J_j term, was the only modification needed to change the uniform density SUMFLD function routine into a triangle density solution.

It should be noted that both programs, UNIFLD and TRIFLD, are set up to solve for $A(\bar{r})$ at a radius $\bar{r}$ from the origin over a range of angles θ. θ is the angle measured down from the z axis to $\bar{r}$. It is much more meaningful to check the solution out over a range such as this, instead of just at one point.

Far-field Evaluation of Test Antenna

Conditions necessary to meet far-field requirements are as follows (2:24):

$$
\begin{aligned}
&r > 2\,L^2/\lambda \\
&r >> L \qquad (24) \\
&r >> \lambda
\end{aligned}
$$

The far-field approximation of the radiation integral was solved with the aid of Fourier transform techniques as follows:

Standard Fourier transform integral form

$$X(\omega) = \int_{-\infty}^{\infty} x(t)\, e^{-j\omega t}\, dt \qquad (25)$$

Far-field radiation integral (3:25)

$$\bar{A}_{ff}(\bar{r}) = \frac{e^{-jk\bar{r}}}{4\pi\bar{r}} \int_{-L/2}^{L/2} \bar{J}(\bar{r}')\, e^{jk\hat{r}\cdot\bar{r}'}\, d\bar{r}' \qquad (26)$$

$$\hat{r} = \hat{x}\sin\theta\cos\phi - \hat{y}\sin\theta\sin\phi + \hat{z}\cos\theta \qquad (27)$$

$$\bar{r}' = \hat{z}' z' \qquad (28)$$

$$\hat{r}\cdot\bar{r}' = z'\cos\theta \qquad (29)$$

let:

$$\psi(\bar{r}) = \frac{e^{-jk\bar{r}}}{4\pi\bar{r}} \qquad (30)$$

$$A_{ff}(\bar{r}) = \hat{z}\,\psi(r)\int_{-L/2}^{L/2} I(z')\, e^{jkz'\cos\theta}\, dz' \qquad (31)$$

let: $u = -k\cos\theta$ (32)

$$A_{ff}(\bar{r}) = \hat{z}\,\psi(r)\int_{-L/2}^{L/2} I(z')\, e^{-juz'}\, dz' \qquad (33)$$

thus:

$$A_{ff}(\bar{r}) = \hat{z}\,\psi(r)\,\mathcal{F}\left[\, I(z')\right] \qquad (34)$$

where $\mathcal{F}[\ ]$ stands for the Fourier Transform

The Fourier transform of the uniform current distribution is:

$$\mathcal{F}\left[I(z')\right] = L\left[\frac{\sin(uL/2)}{(uL/2)}\right] \qquad (35)$$

with
simplifications: L = 1 , x = Ø

$$A_{ff}(\bar{r}) = \hat{z}\,\frac{e^{-jk|y^2+z^2|^{1/2}}}{4\pi\,|y^2+z^2|^{1/2}}\left[\frac{\sin(uL/2)}{(uL/2)}\right] \qquad (36)$$

For far-field

$$\bar{r} > 2L^2/\lambda \Rightarrow \bar{r} > 20.05 \text{ meters} \tag{37}$$

Function routine FARFLD in program UNIFLD (Appendix C) was used to evaluate this expression, for different values of $\bar{r}$. See results in Chapter V.

The same technique was used for the triangular shaped current distribution. Of course, the Fourier Transform of the current density took on a new form:

$$\tilde{\mathcal{F}}\left[I(z')\right] = L/2\left[\frac{\mathrm{SIN}(uL/4)}{(uL/4)}\right]^2 \tag{38}$$

The expression for the vector potential, with the same simplifications as stated before was then:

$$A_{zf}(\bar{r}) = \hat{z}\,\frac{e^{-JK|Y^2+Z^2|^{1/2}}}{4\pi\,|Y^2+Z^2|^{1/2}}\left[\frac{1}{2}\left(\frac{\mathrm{SIN}(uL/4)}{(uL/4)}\right)^2\right] \tag{39}$$

Program TRIFLD contains the function routine FARFLD, which was used to evaluate this expression.

(ICF) Solution of the Test Antenna

The $A(\bar{r})$ expression can be written as follows. (Refer to Figure 8).

$$A(\bar{r}) = \int_{-L/2}^{0} \frac{e^{-jk|Y^2+(z-z')^2|^{1/2}}}{4\pi\,|Y^2+(z-z')^2|^{1/2}}\,dz' \; +$$

$$2\int_{-L/2}^{0} z'\,\frac{e^{-jk|Y^2+(z-z')^2|^{1/2}}}{4\pi\,|Y^2+(z-z')^2|^{1/2}}\,dz' \; +$$

$$\int_{0}^{L/2} \frac{e^{-jk|Y^2+(z-z')^2|^{1/2}}}{4\pi\,|Y^2+(z-z')^2|^{1/2}}\,dz' \; - \tag{40}$$

$$2\int_{0}^{L/2} z'\,\frac{e^{-jk|Y^2+(z-z')^2|^{1/2}}}{4\pi\,|Y^2+(z-z')^2|^{1/2}}\,dz'$$

(with $x = 0$)

To show how the ICF solution goes, let's take a look at

$$I_1 \equiv \int_{0}^{L/2} \frac{e^{-jk|Y^2+(z-z')^2|^{1/2}}}{4\pi\,|Y^2+(z-z')^2|^{1/2}}\,dz' \tag{41}$$

Let u = z - z', then

$$I_1 = \int_{z-L/2}^{z} \frac{e^{-JK|Y^2+u^2|^{1/2}}}{4\pi|Y^2+u^2|^{1/2}}\, du \tag{42}$$

Let u = Y t, then

$$I_1 = \int_{\frac{z-.5}{Y}}^{z/Y} \frac{e^{-JK|1+t^2|^{1/2}}}{4\pi\,|1+t^2|^{1/2}}\, dt \tag{43}$$

Let $w = |1+t^2|^{1/2}$, then

$$I_1 = \int_{|1+(\frac{z-L/2}{Y})^2|^{1/2}}^{|1+(z/Y)^2|^{1/2}} \frac{e^{-JKYw}\, dw}{4\pi\,|w^2-1|^{1/2}} \tag{44}$$

Through these changes of variables, we have transformed the integral into an incomplete cylindrical form. From Agrest and Maksimov, the ICF form is (22:23):

$$\mathcal{E}_{\nu}^{(1)}(c,z) = \frac{2i\,e^{-i2\pi\nu}\,z^{\nu}}{A_{\nu}} \int_{c}^{1} e^{izt}(t^2-1)^{\nu-1/2}\, dt \tag{45}$$

$$A_{\nu} = 2^{\nu}\,\Gamma(\nu+1/2)\,\Gamma(1/2) \tag{46}$$

with $\nu = 0$

$$\mathcal{E}_0^{(1)}(c,z) = \frac{2i}{\pi}\int_c^1 \frac{e^{izt}\,dt}{|t^2-1|^{1/2}} \tag{47}$$

and $z = -ky$ for integral I_1

Following the development of Agrest and Maksimov farther, the form is finally written as follows.

$$E_{\nu}^{\pm}(\omega,z) = \frac{2z^{\nu}}{A_{\nu}}\int_0^{\omega} e^{\pm iz\cos u}\sin^{2\nu} u\,du \tag{48}$$

$$\mathcal{E}_{\nu}^{(1)}(c,z) = E_{\nu}^{+}(-i\cosh^{-1} c, z) \tag{49}$$

This explains how the basic piece of the puzzle for the ICF solution fits into place. The next piece is laid in as follows. It involves the evaluation of the next term in Equation (40).

$$I_2 \equiv -2\int_0^{L/2} z' \frac{e^{-jk|Y^2+(z-z')^2|^{1/2}}}{4\pi|Y^2+(z-z')^2|^{1/2}}\,dz'$$

$$I_2 = -2\left\{-\int_0^{L/2} \frac{(z-z')e^{-jk|Y^2+(z-z')^2|^{1/2}}}{4\pi|Y^2+(z-z')^2|^{1/2}}\,dz' + zI_1\right\} \tag{50}$$

Let $u = z - z'$

$$I_2 = -2\left\{ \int_{z}^{z-L/2} \frac{u\, e^{-jk|Y^2+u^2|^{1/2}}}{4\pi}\, du + z I_1 \right\} \tag{51}$$

Let $t = |Y^2+u^2|^{1/2}$

$$I_2 = -2\left\{ \int_{|Y^2+z^2|^{1/2}}^{|Y^2+(z-L/2)^2|^{1/2}} e^{-jkt}\, dt + z I_1 \right\} \tag{52}$$

So I_2 boils down to a trivial integral plus z times I_1.

A similar progression of steps reveals that the other two terms in Equation (40) can be evaluated with the expressions for I_1 and I_2 with the insertion of a negative value for z.

This is only the preliminary work involved in the ICF solution. It is included here to show how the $A(\bar{r})$ expression is transformed into the ICF form. The earlier statement about needing the uniform current density solution (I_1) is also clarified.

Refer to Appendix D for the remaining steps necessary for the ICF solution. In general terms, the ICF solution used for comparison, is an asymptotic expansion that is restricted to a limited portion of quadrant I ($15^\circ < \theta < 70^\circ$). It turned out to be an extremely useful solution even with this restriction, because it supplied accurate values for $A(\bar{r})$ in both the near- and far-field regions.

In the program UNIFLD (Appendix C), the complex function routine I_1 was used to evaluate the uniform field ICF solution. This was accomplished in two stages, once with a positive value for z, and then again with a negative value. This was done to solve for the current densities both above and below the Y axis, as mentioned before. The necessary additions to function I_1 were added in program TRIFLD (Appendix C, to solve for the triangle distribution.

Chapter IV

Digital Implementation Aspects

Introduction

As with most endeavors embarking on a journey down an unknown path, what is thought to be at the end of the path at the start, may not be there at all. It was certainly the intention at the beginning of this study that the subject area of this chapter would make up the bulk of the work. Only a minimal amount of time however was spent looking into the digital implementation aspect of the problem, due to the effort that was required for the algorithm definition stage.

Most of the time that was spent involved a literature search, looking for the digital algorithms that are needed for the various mathematical operations performed in the radiation integral. This chapter is included more as a source of references for the person carrying on the work for the VLSI implementation of the radiation integral.

Although this study didn't get intimately involved with this aspect of the problem, a good deal of work has been accomplished on the subject by an Air Force Institute of Technology Computer Systems Architecture class (23). The class produced six reports on the digital design aspects of the problem. Anyone interested in reviewing a more indepth treatment is advised to seek out these reports.

Arithmetic Operations Required

A quick glance at the numerical summation solution shows that some very basic mathematical operations are required.

$$A(\bar{r}) \approx \sum_{j=1}^{\wedge\wedge} \frac{\Delta A_j \, e^{-jk|\bar{r}-\bar{r}'_j|}}{4\pi|\bar{r}-\bar{r}'_j|} \tag{53}$$

They are:

multiplication
division
exponential
magnitude

These operations pose no problems whatsoever for the person programming $A(\bar{r})$ on a computer, as was done for the test of the algorithm. How are they accomplished when you don't have the well-established computer language to work with? The language is of course using some form of a digital algorithm to perform the operation. Knowledge of these algorithms was what was required for the digital implementation of the $A(\bar{r})$ numerical expression. Each operation is addressed in the following text.

Multiplication.

Multiplication is probably the most studied and advanced area of all the digital operations next to addition. Only a minimal amount of effort was expended in this area because it was known that there is an abundance of material from which to draw. Already existing floating point processors like (24) are probably the most logical place to start when the final algorithm definition stage is arrived at.

Division.

Division is a much more costly operation in terms of computation time. The literature search located numerous schemes, (25;26;27;28;29;30;31) devised to most efficiently and accurately perform the operation. They range from the simplest, Newton-Raphson iteration (31:278), to quadratic convergence (25:49), to carry look-ahead array dividers (31:296). All the schemes turn the division into some form of multiplication and division. The time spent in this area of the digital math produced the following results. The simplicity and directness of the Newton-Raphson method made it a desirable approach to use. A good deal more time and effort is required to understand the other methods at the same level in order to make a meaningful comparison. Unfortunately that time was not spent during this study, so no recommendations can be given. It's conceivable, as a matter of fact, to spend an entire study effort testing out the various methods in relationship to the numerical radiation integral solution. A good place to start is with the class project reports.

Exponential.

The first algorithm found to evaluate the exponential (32:71) was a polynomial expansion. After working with the expansion, it was noted (33) that due to the complex nature of the exponential, the expansion was the combination of the expansions for the sine and cosine functions. With this realization, a more efficient algorithm known as the Cordic Trigonometric Computing Technique (34:330) was investigated.

Reference (35:1283) goes into an actual hardware build-up of the Cordic algorithm. Reference (36:144) updates the 1959 algorithm for modern VLSI applications. All the research done in this area points towards breaking the exponential up into sine and cosines, then using this Cordic algorithm to perform the operation digitally.

Magnitude.

Calculation of the magnitude of vector $|\bar{r} - \bar{r}'|$, boils down to a combination of addition, subtraction, multiplication, and a square root:

$$|(X-X')^2 + (Y+Y')^2 + (Z-Z')^2|^{1/2} \qquad (54)$$

The square root algorithm was the last one to seek out in order to have a full set of digital algorithms that performed the math of the $A(\bar{r})$ numerical expression.

Initial findings of this search found that the square root function can be evaluated with the Newton-Raphson method in much the same manner as division. The method goes like this:

Basic Newton-Raphson formula to find the root of an equation (37:463)

$$x_{n+1} = x_n - \frac{f(x_n)}{f'(x_n)} \tag{55}$$

where:

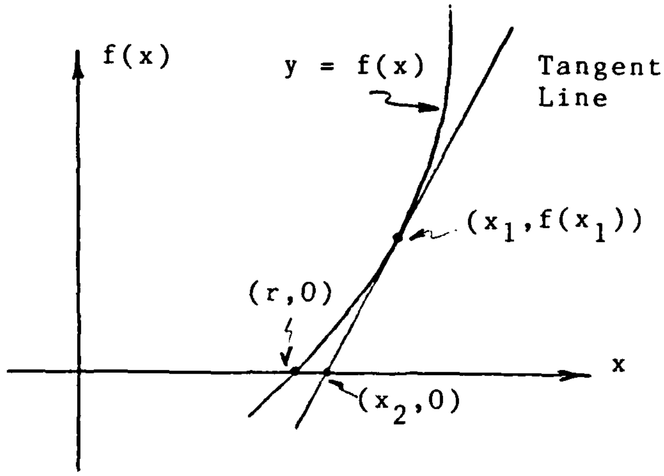

Figure 1Ø

Approximation of f(x) = Ø with tangent line

Now look at square root

Want:

$$A = \sqrt{x}$$

$$A^2 = x \tag{56}$$

$$A^2 - x = 0$$

To put into Newton-Raphson form

Let: $x_n^2 - x = f(x_n)$, where $f(x_n)$ approaches zero

over the progression of steps.

then:

$$f'(x_n) = 2x_n \tag{57}$$

thus:

$$x_{n+1} = x_n - \frac{x_n^2 - x}{2x_n} = .5\left(x_n + \frac{x}{x_n}\right) \tag{58}$$

Once again, a seemingly difficult process such as a square root, has been converted into an addition and a multiplication. The only complication is that care must be taken in assigning the first guess $x_\emptyset$, so that the process converges down to within an specified ϵ away from the actual answer. The method is straightforward to implement digitally. Other methods exist (38;39) as examples, that are probably more efficient. Locating an algorithm to perform the math digitally is not the problem, but rather choosing which one to use. The similarity between the divide algorithm and the square root algorithm does not end with the Newton-Raphson scheme, so the research accomplished for division will also be useful for the square root.

General Processor Block Diagram

This chapter would not be complete without some mention of the basic digital architecture that the processor will assume. The algorithms that perform the math will have to have someplace to call home, and will have a significant role in defining what home looks like. Figure 11 shows the basic concept.

The first thing that probably catches one's eye, is what is this host computer? There is no need to reinvent the wheel and design a complete stand alone computer that evaluates the radiation integral. It is more prudent to design the $A(\bar{r})$ processor so that it will work in conjunction with an existing computer unit. This computer unit might be as sophisticated as a large main-frame, or as simple as a microprocessor. This is a question that will have to be addressed in the digital implementation stage. The duties of this host computer will include such things as: loading the $A(\bar{r})$ processor's memory with the current densities, point locations,and wave number; plotting out graphs.

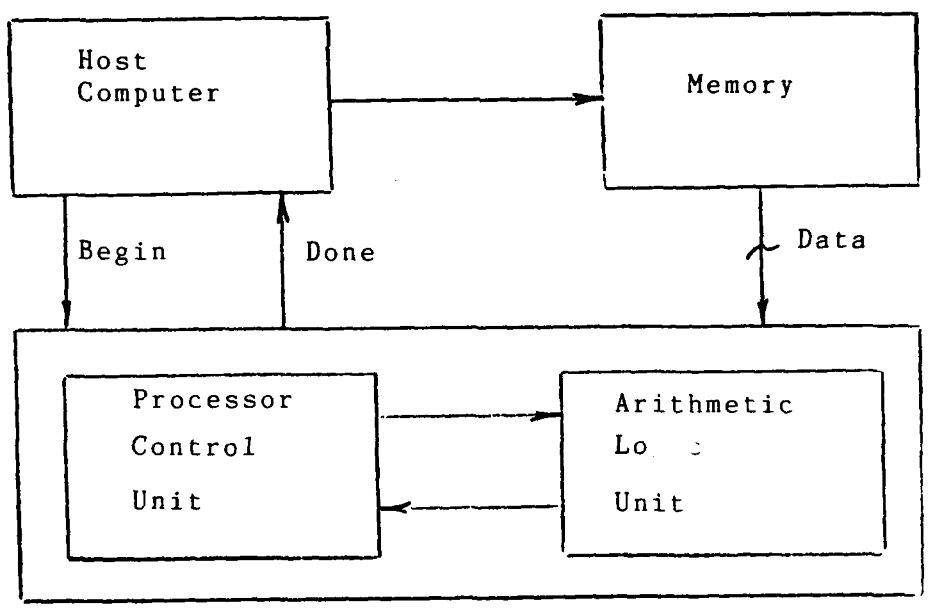

Figure 11

Basic Processor Block Diagram

The memory unit is quite simply just that, the storage location for all the data inputs to the processor. Even through simple sounding in concept, there are several questions to be resolved here also. First, what is the size of this memory? That question can't be fully answered until the accuracy of the final $A(\bar{r})$ processor, or more realistically the E and H processors, is defined. Accuracy and memory size go hand in hand because the number of subdivisions the antenna is broken up into is a direct measure of the accuracy of the solution. Based on the answer to the size question, the question of where does this memory physically exist can be investigated. Is it part of the host computer, or a separate memory box built in conjuction with the $A(\bar{r})$ processor?

It only makes sense, that on board the processor unit are the smarts to take over control of the calculations, once the host has said the memory is loaded, begin. The control unit will take charge of the operation, and direct the arithmetic/logic unit (ALU) in the calculation of sines and square roots, etc. Two of the basic time-saving concepts are to pipeline parallel ALU units. The control unit will be in charge of these operations. Calculation of the various values in the magnitude calculation, such as $(x - x')^2$ etc, can be accomplished for successive parts of the antenna, while the square root processor is working on a specific point. These values can be stacked up in the pipeline awaiting their turn in the magnitude processor.

This is just one of the examples of how pipelining can be used to speed up the calculation.

The basic electromagnetic nature of the solution has broken the calculation up into three scalar equations (3:11), one each for the x,y, and z space coordinates. It will therefore be likely to have the one control unit in charge of three separate/parallel ALU units.

Going still deeper to take a macroscopic look at the ALU units, one will find a noteworthy beast. Addition and multiplication form the basis for all the mathematical operations needed for the calculation of $A(\bar{r})$. A decision based on a time versus cost analysis, will have to be made about the parallelism of the ALU unit itself. It can consist of one unit that performs the necessary steps one at a time, or a number of mini-processors that evaluates the sine, magnitude, etc. in parallel.

There are still a lot of questions to be answered, even though many problem areas have been examined. With regards to the digital implementation aspect, it appears that all the mathematical operations can be performed quite easily with the basic algorithms. A good deal more effort will be required to pick and choose the most efficient algorithms to work in conjunction with the pipelined parallel processors to yield the final solution. Before any indepth work can be accomplished in this area, such as number representation or register definition etc., the algorithms that solve for the E and H fields must be defined. See the recommendation section of Chapter V for a full explanation.

Chapter V

Results, Conclusions, Recommendations

Comparison of Results

Table I and Figures 12 through 15 (this chapter) show representative results obtained from the triangular current distribution. Tables II through XIV (Appendix E) list results from both the uniform and the triangular distributions for different values of M and $\bar{r}$.

The comparison was conducted in a limited portion of quadrant I, at various distances $\bar{r}$, from the origin. Values for $A(\bar{r})$ were calculated at the radius $\bar{r}$, that swept over the test range, in increments of the angle θ ($15^\circ < \theta < 70^\circ$). θ is the angle measured from the z axis down to the radius vector $\bar{r}$. This limitation was brought on by the complexity of the ICF solution. The ICF solution turned out to be fairly expensive in terms of work involved, but was an extremely useful closed form solution to have for the comparison process. The nature of the solution required that the space the antenna radiates into be broken up into a number of asymptotic regions. It was decided that only the asymptotic expansion of the ICF for the above portion of quadrant I was necessary, because the symmetry of the antenna made the solution of $A(\bar{r})$ in the other quadrants mirror images of quadrant I. This portion of quadrant I was more than an adequate test range to make or break the numerical solution. A check outside this region, θ equal zero degrees, was also conducted to make sure the numerical solution responded with the expected result. The vector potential at this observation point is zero, and that is exactly what the numerical solution produced.

The check of the numerical approximation against the other two solutions was accomplished by comparing the number of matching digits of the magnitude values of $A(\bar{r})$ for different values of M. The comparison was accomplished in this manner, because once M was sufficiently large ($M > 200$), it was virtually impossible to graph the differences over the dynamic range of θ tested. It also did not seem appropriate to convert the comparison values into decibels (dB's), which is a common practice in similar studies, as the numbers represented the vector potential, not the E or H fields.

More attention was paid to the results of the comparison conducted for the triangular distribution. This was based on the thought that the triangular distribution provided a more complex and realistic study upon which to judge the test. Results from the uniform distribution were used more to check the trends noted from the triangle distribution.

There were several areas of interest: how large did M have to be to yield accurate results; what were accurate results; did the numerical solution work in both the near- and far-field regions? A ballpark estimate of how large M has to be can be obtained by making sure that h (h = L / M) is less than one tenth of the wavelength ($h < .1 \lambda$) radiating from the antenna. For the values used in the test case ($\lambda \sim .1$ meter), the estimate figured out to, h <.01 meter, or M > 100. Tests were therefore run with values of M equalling 50, 100, 200, and 500. Sure enough, results from M = 50 were poor, marginal for M = 100, and reassuringly accurate for M = 500. Accuracy here meant a match of approximately three digits between the $A(\bar{r})$ magnitude values of the numerical solution and the ICF solution. This is a rather simplistic approach, but will be born out in the recommendation section as an adequate measure for this stage in the development of the processor.

The final check of the numerical solution, was to see if it worked in the near- and far-field regions. A check of Tables I and X shows that when M is sufficiently large, the numerical solution yields just as accurate results in close to the antenna as it does in the far-field region.

The far-field solution was the first form of a comparison solution secured, but was limited to the far-field, and experienced phase error around the null points. What might have been thought to be an error in the numerical solution at these points was shown to be a far-field error with the aid of the ICF solution. The far-field solution was therefore only used as an initial check of the numerical and ICF solutions, to see if they were on the right track.

Table I

THETA (DEG)	MAGNITUDE OF VECTOR POTENTIAL		
	TRIANGULAR CURRENT DISTRIBUTION		
	R = 50.0	M = 200	K = 63.
	FAR-FIELD	ICF	NUMERICAL
15.0	0.7748E-06	0.7752E-06	0.7746E-06
18.0	0.1573E-05	0.1574E-05	0.1564E-05
21.0	0.2620E-05	0.2621E-05	0.2613E-05
24.0	0.3606E-05	0.3607E-05	0.3591E-05
27.0	0.3997E-05	0.3997E-05	0.3984E-05
30.0	0.3304E-05	0.3302E-05	0.3288E-05
33.0	0.1638E-05	0.1636E-05	0.1630E-05
36.0	0.1497E-06	0.1877E-06	0.1868E-06
39.0	0.5458E-06	0.5746E-06	0.5674E-06
42.0	0.3347E-05	0.3351E-05	0.3342E-05
45.0	0.6289E-05	0.6286E-05	0.6269E-05
48.0	0.5771E-05	0.5762E-05	0.5747E-05
51.0	0.1774E-05	0.1778E-05	0.1775E-05
54.0	0.2570E-06	0.5693E-06	0.5704E-06
57.0	0.6069E-05	0.6087E-05	0.6080E-05
60.0	0.1283E-04	0.1281E-04	0.1280E-04
63.0	0.9049E-05	0.9012E-05	0.9006E-05
66.0	0.2915E-06	0.1180E-05	0.1181E-05
69.0	0.8882E-05	0.9064E-05	0.9060E-05

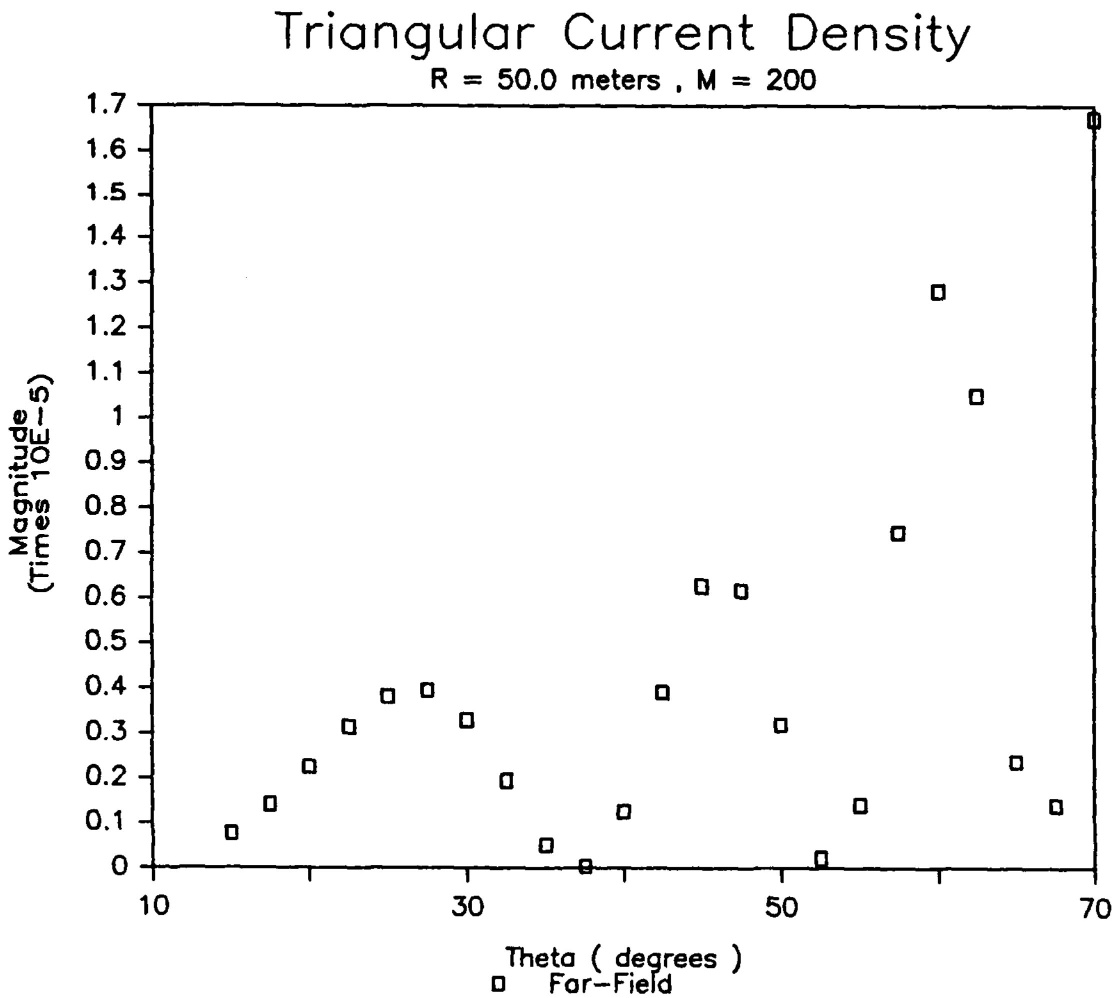

Figure 12
Magnitude of Vector Potential (Far-Field)

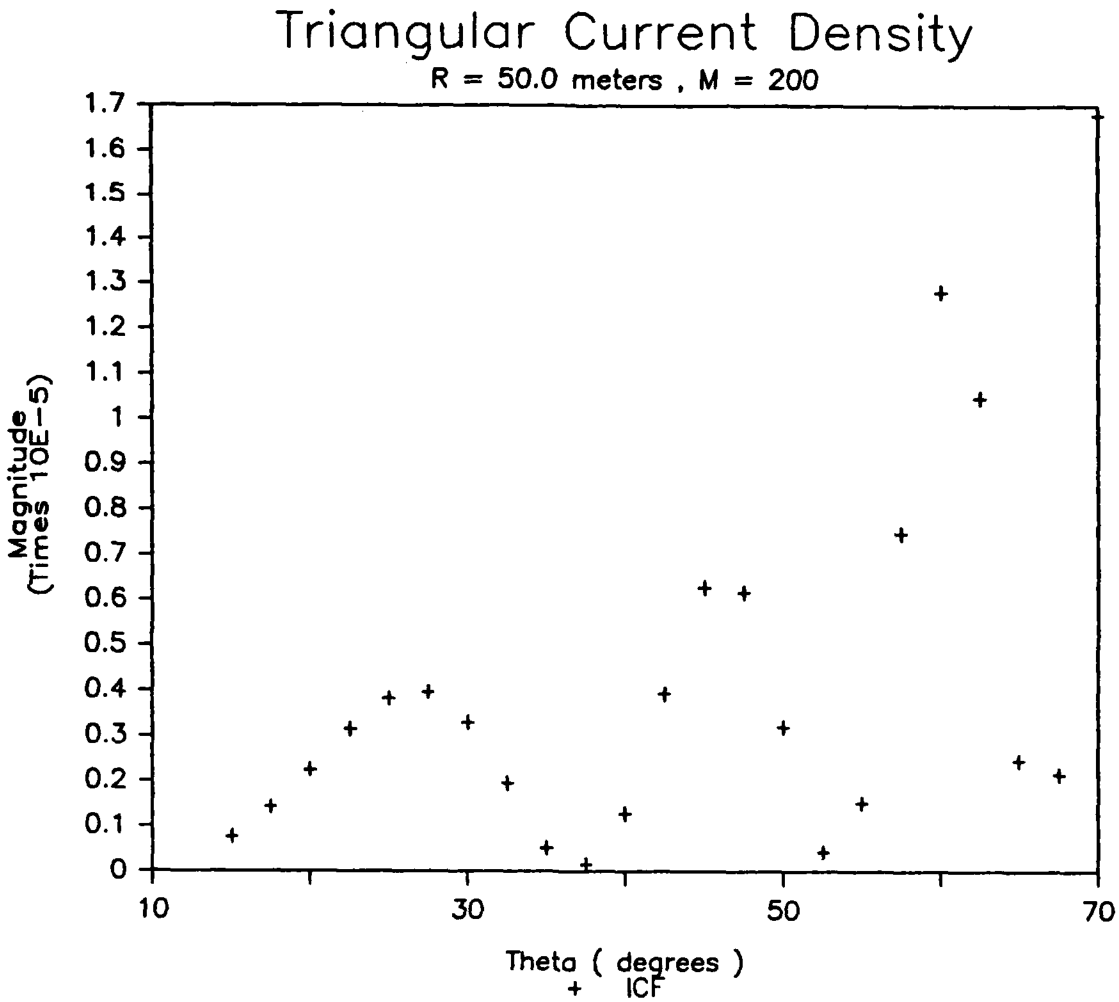

Figure 13
Magnitude of Vector Potential (ICF)

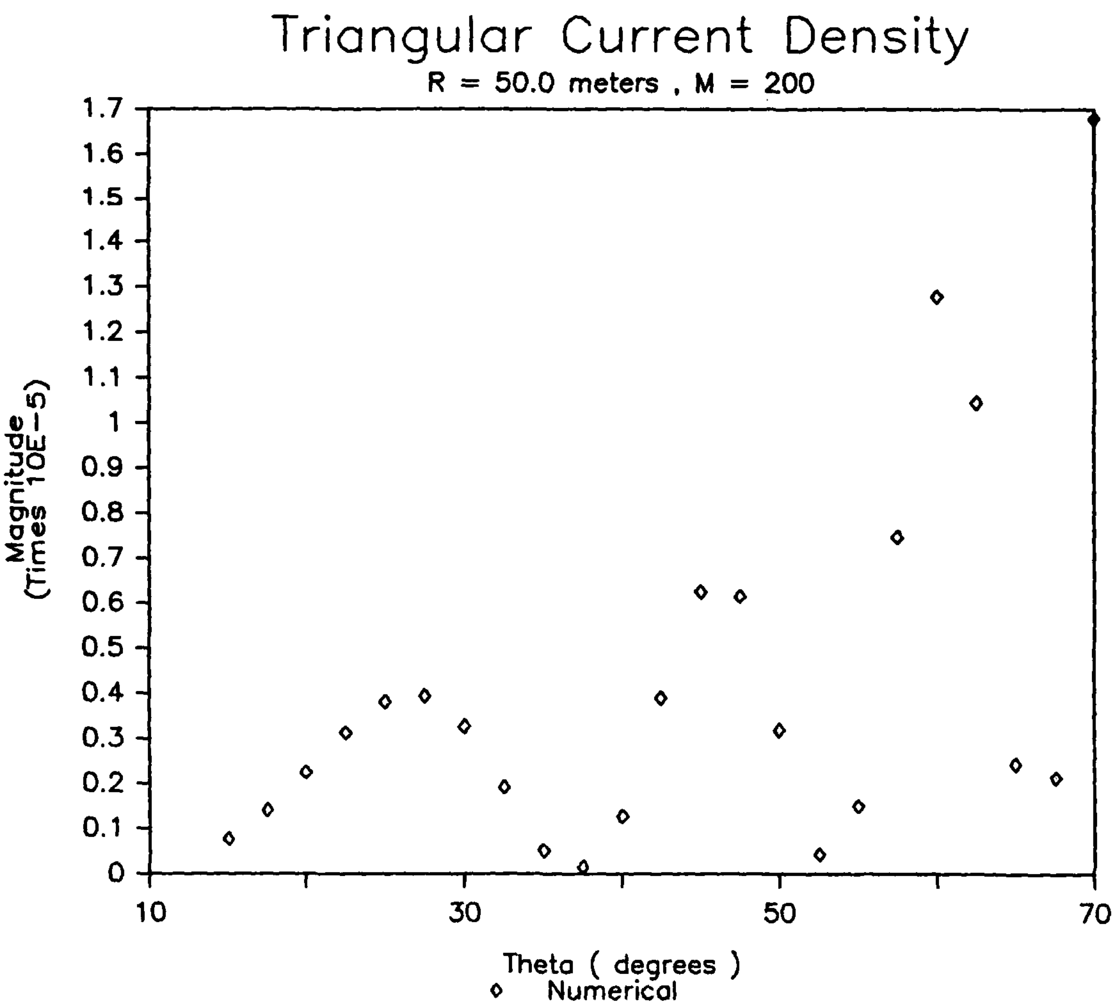

Figure 14
Magnitude of Vector Potential (Numerical)

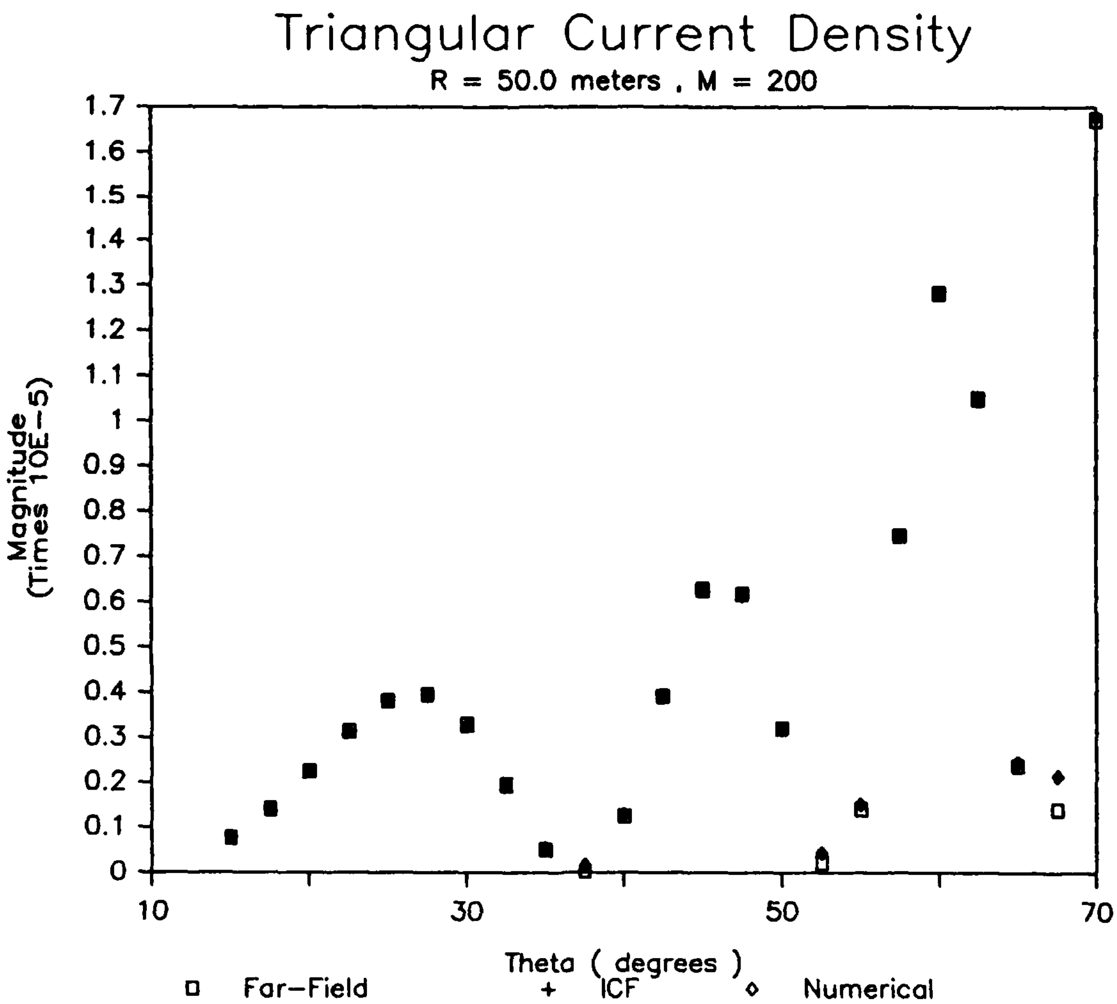

Figure 15
Magnitude of Vector Potential
(Far-field, ICF, Numerical)

Conclusions

These were satisfying results. First of all, the solution worked equally well in both the near- and far-field. This was one of the major constraints stated back at the beginning of the project. Secondly, the solution was spilling out accurate results for peanuts. A value of 500 for M was well within the realm of feasibility. Even the software used for the test had no time difficulties with M at this value. M could certainly be increased by an order of magnitude to yield even more accurate results, and experience no major time problems.

The method once too crude to even consider, had come through this initial check with flying colors. It actually produced sound values for $A(\bar{r})$, without experiencing the difficulties of the other two methods around the null points and asymptotic lines spoken of earlier.

The mathematical form of the solution is also very appealing. All the algorithms necessary for digital implementation, like divide, sine, cosine, etc., exist. The solution works and can be embedded in a VLSI chip.

Recommendations

The solution has been shown to work for the simplest of one-dimensional antennas. The obvious next steps would be to press on to a two-dimensional antenna in a convenient plane, like the yz plane, and then to a two-dimensional antenna located arbitrarily in space. The problems spoken of earlier, about securing a known closed form solution for the comparatively simple one-dimensional case, were only magnified by the attempt to go to higher dimensional cases. This study had come to the close of its time period, and it was felt this recommendation section would lead the reader off in a search for these closed form comparison solutions. It was right at this twilight stage in the study, that another piece of information was learned that solved the problem of locating the closed form solutions for $A(\bar{r})$.

Back on page one, it was stated that the accepted mathematical way to find the E and H fields, is to first solve for $A(\bar{r})$. The process involves taking a derivative of A to solve for H and then another derivative of H to yield E. It turns out that when one is using numerical methods to attack a problem, some rather disastrous results can occur if proper care is not given to the sequence of steps. Numerical integration involves dividing the area to be integrated up into segments, and performing a series of summations. Numerical differentiation also breaks the region up into segments, and evaluates the slope between the segments. If both operations are to be performed on a given expression, the segment width of the differentiation must be wider than that for the integration, or the numerical differentiation can yield invalid results. No such problems arise from a reverse in the sequence of operations, differentiation before integration. It is therefore wiser to perform differentiation first. The results of the $A(\bar{r})$ numerical summation algorithm can be used as the basis for the next stage of development, that is to look into the problem of bringing the ∇X into the integral before the integration is performed. Some of the problems to be solved are: do you stay with Cartesian Coordinates; how do you deal with the general shape antenna problem; does the summation algorithm keep the same basic form so these initial results can be used?

It is felt at this time, that the algorithm will keep the same basic form. Once this fact is born out, more indepth and accurate testing of the algorithm can be performed. It would be premature to start looking into the number of binary bits necessary for a specified accuracy, etc., until the final algorithm is defined.

Mention should also be made at this point about another possible cause for concern. During this whole analysis period it has been assumed that the current density input values could be acquired from somewhere. This somewhere might be the output from a numerical technique like a method of moments program, or the data base from the physical measurement of an existing antenna. It has been stated in this document, that the larger the number of sub-elements the antenna is broken up into, the more accurate the solution. In order to obtain the desired accuracy for complex antenna shapes, it may prove to be a real challenge to actually come up with the current density inputs. A processor that can quickly and accurately produce electric or magnetic fields won't be of much use if there are only trivial input current densities to work with. It is also therefore suggested that some research be devoted to this area of how and where to obtain these inputs.

There is a good deal of work left to get to the climax, a set of silicon chips. It is hoped that this documentation of the initial attempts will allow the person or persons carrying on the work to progress at a more rapid rate. Good Luck.

Appendix A

Three-Dimensional Expansion of Two Numerical Integration Schemes

The one-dimensional Simpson's Rule:

$$\int_a^b f(x)dx \approx \frac{h}{3}\left[f(a) + 2\sum_{j=1}^{m-1} f(x_{2j}) + 4\sum_{j=1}^{m} f(x_{2j-1}) + f(b)\right] \tag{59}$$

is expanded out into three-dimensions

$$\int_a^b \int_c^d \int_e^f f(x,y,z)\, dz\, dy\, dx \Rightarrow 64 \text{ TERMS} \tag{60}$$

The function inside the integrals is changed to:

$$\int_a^b \int_c^d \int_e^f f(x,y,z) \text{ SIN } K \text{ [illegible]} \tag{61}$$

A modified Simpson's rule that deals with these types of functions, known as Filon's method is expanded out into three dimensions. The resulting expansion yields 216 terms. Only a representative number of these terms are included in this appendix.

$$\int_a^b \int_c^d \int_e^f f(x,Y,z)\,dz\,dY\,dx$$

EXPAND SIMPSON'S RULE SOLUTION OUT INTO THREE-DIMENSIONS

$$\int_e^f f(x,Y,z)\,dz \approx \frac{g}{3}\Big[f(x,Y,e) + 2\sum_{j=1}^{M-1} f(x,Y,z_{2j})$$

$$+ 4\sum_{j=1}^{M} f(x,Y,z_{2j-1}) + f(x,Y,f)\Big]$$

$$\int_c^d f(x,Y,z_j)\,dY \approx \frac{h}{3}\Big[f(x,c,z_j) + 2\sum_{i=1}^{N-1} f(x,Y_{2i},z_j)$$

$$+ 4\sum_{i=1}^{N} f(x,Y_{2i-1},z_j) + f(x,d,z_j)\Big]$$

$$\int_a^b f(x,Y_i,z_j)\,dx \approx \frac{W}{3}\Big[f(a,Y_i,z_j) + 2\sum_{k=1}^{P-1} f(x_{2k},Y_i,z_j)$$

$$+ 4\sum_{k=1}^{P} f(x_{2k-1},Y_i,z_j) + f(b,Y_i,z_j)\Big]$$

THIS FINAL EXPRESSION IS EXPANDED OUT IN TERMS OF Y_i AND z_j, TO YIELD 64 TERMS.

(EIGHT NON-SUMMATION TERMS)

$$f(a,c,e) + f(a,c,f) + f(a,d,e)$$
$$+ f(a,d,f) + f(b,c,e) + f(b,c,f)$$
$$+ f(a,d,e) + f(a,d,f)$$

(24 SINGLE SUMMATION TERMS)

$$2\sum_{k=1}^{P-1} f(x_{2k}, c, e) + 4\sum_{k=1}^{P} f(x_{2k-1}, c, e)$$

$$+ 2\sum_{k=1}^{P-1} f(x_{2k}, c, f) + 4\sum_{k=1}^{P} f(x_{2k-1}, c, f)$$

$$+ 2\sum_{k=1}^{P-1} f(x_{2k}, d, e) + 4\sum_{k=1}^{P} f(x_{2k-1}, d, e)$$

$$+ 2\sum_{k=1}^{P-1} f(x_{2k}, d, f) + 4\sum_{k=1}^{P} f(x_{2k-1}, d, f)$$

$$+ 2\sum_{i=1}^{N-1} f(a, Y_{2i}, e) + 4\sum_{i=1}^{N} f(a, Y_{2i-1}, e)$$

$+ \rightarrow$

$$+ 2\sum_{i=1}^{N-1} f(a, Y_{2i}, f) + 4\sum_{i=1}^{N} f(a, Y_{2i-1}, f)$$

$$+ 2\sum_{i=1}^{N-1} f(b, Y_{2i}, e) + 4\sum_{i=1}^{N} f(b, Y_{2i-1}, e)$$

$$+ 2\sum_{i=1}^{N-1} f(b, Y_{2i}, f) + 4\sum_{i=1}^{N} f(b, Y_{2i-1}, f)$$

$$+ 2\sum_{j=1}^{M-1} f(a, c, z_{2j}) + 4\sum_{j=1}^{M} f(a, c, z_{2j-1})$$

$$+ 2\sum_{j=1}^{M-1} f(a, d, z_{2j}) + 4\sum_{j=1}^{M} f(a, d, z_{2j-1})$$

$$+ 2\sum_{j=1}^{M-1} f(b, c, z_{2j}) + 4\sum_{j=1}^{M} f(b, c, z_{2j-1})$$

$$+ 2\sum_{j=1}^{M-1} f(b, d, z_{2j}) + 4\sum_{j=1}^{M} f(b, d, z_{2j-1})$$

(24 DOUBLE SUMMATION TERMS)

$$4\sum_{k=1}^{P-1}\sum_{i=1}^{N-1} f(X_{2k}, Y_{2i}, e) + 8\sum_{k=1}^{P-1}\sum_{i=1}^{N} f(X_{2k}, Y_{2i-1}, e)$$

$$+ 8\sum_{k=1}^{P}\sum_{i=1}^{N-1} f(X_{2k-1}, Y_{2i}, e) + 16\sum_{k=1}^{P}\sum_{i=1}^{N} f(X_{2k-1}, Y_{2i-1}, e)$$

$$+ 4\sum_{k=1}^{P-1}\sum_{i=1}^{N-1} f(X_{2k}, Y_{2i}, f) + 8\sum_{k=1}^{P-1}\sum_{i=1}^{N} f(X_{2k}, Y_{2i-1}, f)$$

$$+ 8\sum_{k=1}^{P}\sum_{i=1}^{N-1} f(X_{2k-1}, Y_{2i}, f) + 16\sum_{k=1}^{P}\sum_{i=1}^{N} f(X_{2k-1}, Y_{2i-1}, f)$$

$$+ 4\sum_{k=1}^{P-1}\sum_{j=1}^{M-1} f(X_{2k}, c, Z_{2j}) + 8\sum_{k=1}^{P-1}\sum_{j=1}^{M} f(X_{2k}, c, Z_{2j-1})$$

$$+ 8\sum_{k=1}^{P}\sum_{j=1}^{M-1} f(X_{2k-1}, c, Z_{2j}) + 16\sum_{k=1}^{P}\sum_{j=1}^{M} f(X_{2k-1}, c, Z_{2j-1})$$

$$+ 4\sum_{k=1}^{P-1}\sum_{j=1}^{M-1} f(X_{2k}, d, Z_{2j}) + 8\sum_{k=1}^{P-1}\sum_{j=1}^{M} f(X_{2k}, d, Z_{2j-1})$$

$$+ 8\sum_{k=1}^{P}\sum_{j=1}^{M-1} f(X_{2k-1}, d, Z_{2j}) + 16\sum_{k=1}^{P}\sum_{j=1}^{M} f(X_{2k-1}, d, Z_{2j-1})$$

$+ \longrightarrow$

$$+4\sum_{i=1}^{N-1}\sum_{j=1}^{M-1} f(a, Y_{2i}, Z_{2j}) \quad +8\sum_{i=1}^{N-1}\sum_{j=1}^{M} f(a, Y_{2i}, Z_{2j-1})$$

$$+8\sum_{i=1}^{N}\sum_{j=1}^{M-1} f(a, Y_{2i-1}, Z_{2j}) \quad +16\sum_{i=1}^{N}\sum_{j=1}^{M} f(a, Y_{2i-1}, Z_{2j-1})$$

$$+4\sum_{i=1}^{N-1}\sum_{j=1}^{M-1} f(b, Y_{2i}, Z_{2j}) \quad +8\sum_{i=1}^{N-1}\sum_{j=1}^{M} f(b, Y_{2i-1}, Z_{2j-1})$$

$$+8\sum_{i=1}^{N}\sum_{j=1}^{M-1} f(b, Y_{2i-1}, Z_{2j}) \quad +16\sum_{j=1}^{N}\sum_{j=1}^{M} f(b, Y_{2i-1}, Z_{2j-1})$$

(EIGHT TRIPLE SUMMATION TERMS)

$$8\sum_{k=1}^{P-1}\sum_{i=1}^{N-1}\sum_{j=1}^{M-1} f(X_{2k}, Y_{2i}, Z_{2j}) \quad +$$

$$+\ 16\sum_{k=1}^{P-1}\sum_{i=1}^{N-1}\sum_{j=1}^{M} f(X_{2k}, Y_{2i}, Z_{2j-1}) \quad +$$

$$+\ 16\sum_{k=1}^{P}\sum_{i=1}^{N-1}\sum_{j=1}^{M-1} f(X_{2k-1}, Y_{2i}, Z_{2j}) \quad +$$

$$+\ 32\sum_{k=1}^{P}\sum_{i=1}^{N-1}\sum_{j=1}^{M} f(X_{2k-1}, Y_{2i}, Z_{2j-1}) \quad + \quad \rightarrow$$

$$+ 16\sum_{k=1}^{P-1}\sum_{i=1}^{N}\sum_{j=1}^{M-1} f(X_{2k}, Y_{2i-1}, Z_{2j}) +$$

$$+ 32\sum_{k=1}^{P-1}\sum_{i=1}^{N}\sum_{j=1}^{M} f(X_{2k}, Y_{2i-1}, Z_{2j-1}) +$$

$$+ 32\sum_{k=1}^{P}\sum_{i=1}^{N}\sum_{j=1}^{M-1} f(X_{2k-1}, Y_{2i-1}, Z_{2j}) +$$

$$+ 64\sum_{k=1}^{P}\sum_{i=1}^{N}\sum_{j=1}^{M} f(X_{2k-1}, Y_{2i-1}, Z_{2j-1})$$

THE SUMMATION OF ALL 64 TERMS IS MULTIPLIED

BY $\frac{Whg}{27}$ FOR THE FINAL SOLUTION.

$$\int_a^b \int_c^d \int_e^f f(X,Y,Z) \sin K(X,Y,Z)\, dX\, dY\, dZ$$

EXPAND FILON'S METHOD OUT INTO THREE-DIMENSIONS

$$\int_a^b f(X,Y,Z) \sin K(X,Y,Z)\, dX \approx$$

$$h\Big\{ \alpha_X\big[f(a,Y,Z) \cos K(a,Y,Z) -$$

$$f(b,Y,Z) \cos K(b,Y,Z)\big] +$$

$$\beta_X\Big[f(a,Y,Z) \sin K(a,Y,Z) +$$

$$2\sum_{k=1}^{p-1} f(X_{2k},Y,Z) \sin K(X_{2K},Y,Z)$$

$$+ f(b,Y,Z) \sin K(b,Y,Z)\Big] +$$

$$\gamma_X \sum_{k=1}^{p} f(X_{2k-1},Y,Z) \sin K(X_{2k-1},Y,Z) \Big\}$$

THESE SIX TERMS ARE EXPANDED OUT IN Y AND Z IN A SIMILIAR FASHION AS THAT USED FOR THE PROCEEDING SIMPSON RULE EXPANSION, TO YIELD A TOTAL OF 216 TERMS. THE FOLLOWING IS A REPRESENTATIVE EXAMPLE OF THE TOTAL EXPANDED TERMS.

$$\alpha_Z \alpha_Y \alpha_X f(a,d,e) \sin K(a,d,e)$$

$$-\alpha_Z \alpha_Y \alpha_X f(b,d,e) \sin K(b,d,e)$$

$$+2\alpha_Z \alpha_Y B_X \sum_{k=1}^{P-1} f(X_{2k},d,e) \sin K(X_{2k},d,e)$$

$$+\alpha_Z \alpha_Y \gamma_X \sum_{k=1}^{P} f(X_{2k-1},d,e) \sin K(X_{2k-1},d,e)$$

$$+2\alpha_Z B_Y \alpha_X \sum_{i=1}^{N-1} f(b,Y_{2i},e) \sin K(b,Y_{2i},e)$$

$$-2\alpha_Z B_Y \alpha_X \sum_{i=1}^{N-1} f(a,Y_{2i},e) \sin K(a,Y_{2i},e)$$

$$+2\alpha_Z B_Y B_X \sum_{i=1}^{N-1} f(b,Y_{2i},e) \cos K(b,Y_{2i},e)$$

$$+2\,\alpha_Z\,\beta_Y\,\gamma_X \sum_{i=1}^{N-1}\sum_{k=1}^{P} f(X_{2k-1}, Y_{2i}, e)\,\cos K(X_{2k-1}, Y_{2i}, e)$$

+ (ETC.)

(EIGHT TRIPLE SUMMATION TERMS)

$$8\,\beta_Z\,\beta_Y\,\beta_X \sum_{j=1}^{M-1}\sum_{i=1}^{N-1}\sum_{k=1}^{P-1} f(X_{2k}, Y_{2i}, Z_{2j})\,\sin K(X_{2k}, Y_{2i}, Z_{2j})$$

$$+4\,\beta_Z\,\beta_Y\,\gamma_X \sum_{j=1}^{M-1}\sum_{i=1}^{N-1}\sum_{k=1}^{P} f(X_{2k-1}, Y_{2i}, Z_{2j})\,\sin K(X_{2k-1}, Y_{2i}, Z_{2j})$$

$$+4\,\beta_Z\,\gamma_Y\,\beta_X \sum_{j=1}^{M-1}\sum_{i=1}^{N}\sum_{k=1}^{P-1} f(X_{2k}, Y_{2i-1}, Z_{2j})\,\sin K(X_{2k}, Y_{2i-1}, Z_{2j})$$

$$+2\,\beta_Z\,\gamma_Y\,\gamma_X \sum_{j=1}^{M-1}\sum_{i=1}^{N}\sum_{k=1}^{P} f(X_{2k-1}, Y_{2i-1}, Z_{2j})\,\sin K(X_{2k-1}, Y_{2i-1}, Z_{2j})$$

$$+4\,\gamma_Z\,\beta_Y\,\beta_X \sum_{j=1}^{M}\sum_{i=1}^{N-1}\sum_{k=1}^{P-1} f(X_{2k}, Y_{2i}, Z_{2j-1})\,\sin K(X_{2k}, Y_{2i}, Z_{2j-1})$$

$$+2\,\gamma_Z\,\beta_Y\,\gamma_X \sum_{j=1}^{M}\sum_{i=1}^{N-1}\sum_{k=1}^{P} f(X_{2k-1}, Y_{2i}, Z_{2j-1})\,\sin K(X_{2k-1}, Y_{2i}, Z_{2j-1})$$

$+ \rightarrow$

$$+ 2\, \gamma_Z\, \gamma_Y\, B_X \sum_{j=1}^{M} \sum_{i=1}^{N} \sum_{k=1}^{P-1} f(X_{2k}, Y_{2i-1}, Z_{2j-1}) \sin K(X_{2k}, Y_{2i-1}, Z_{2j-1})$$

$$+ \gamma_Z\, \gamma_Y\, \gamma_X \sum_{j=1}^{M} \sum_{i=1}^{N} \sum_{k=1}^{P} f(X_{2k-1}, Y_{2i-1}, Z_{2j-1}) \sin K(X_{2k-1}, Y_{2i-1}, Z_{2j-1})$$

THE SUMMATION OF ALL 216 TERMS IS MULTIPLIED BY whg FOR THE FINAL SOLUTION.

Appendix B

Numerical Integration and Closed Form Solution Comparison of a Special Integrand Function

Figure 4b shows the special function to be integrated between limits a and b. It consists of the combination of a slowly oscillating term (cos (π z / 3)) and a rapidly oscillating term (cos (k z)). Two closed form solutions are needed for the comparison, they are (F & G):

$$F = \int_{a+h}^{b-h} \cos(\pi z/3)\cos(kz)\,dz \tag{62}$$

$$F = \int_{a+h}^{b-h} \cos(\pi z/3 + kz)\,dz + \int_{a+h}^{b-h} \cos(\pi z/3 - kz)\,dz \tag{63}$$

Let k = 63.

F = - 0.01477

(This is the solution of the integral minus the end points)

$$G = \int_{-1}^{1} \cos(\pi z/3)\cos(kz)\,dz \tag{64}$$

with k = 63. Again

G = 0.00246

This is the solution of the integral over the entire region, (- 1 to 1)

Program TSTFLN at the end of this appendix was used to calculate the same two integrals using Filon's numerical integration method.

$$\int_a^b f(z)\cos(kz)\,dz \approx$$

$$h\Big\{\alpha\big[f(b)\sin(kb) - f(a)\sin(ka)\big] +$$

$$\beta\big[f(a)\cos(ka) + f(b)\cos(kb)\big] + \tag{65}$$

$$\beta\sum_{j=1}^{M-1} f(z_{2j})\cos(kz_{2j}) +$$

$$\gamma\sum_{j=1}^{M} f(z_{2j-1})\cos(kz_{2j-1})\Big\}$$

where:

$$\alpha = \frac{2}{45}\theta^3 - \frac{2}{315}\theta^5 + \cdots$$

$$\beta = \frac{2}{3} + \frac{2}{15}\theta^2 - \frac{4}{105}\theta^4 + \cdots$$

$$\gamma = \frac{4}{3} - \frac{2}{15}\theta^2 + \frac{2}{210}\theta^4 + \cdots \tag{66}$$

$$\theta = kh$$

$$h = (b-a)/2M$$

The first four terms of this expression deal only with the end points (a and b). The two summations provide the solution for all points in between the end points.

The comparison consisted of checking to see if the two summation terms in Filon's method would equal the closed form solution for the same interval. Output from program TSTFLN, ANSHRT, is the numerical integration's solution for this middle interval. The closed form solution F and ANSHRT are in complete disagreement. To check that the value ANSHRT is correct, program TSTFLN also calculates Filon's values at the end points, and adds this quantity to ANSHRT. Solution FULFLN in program TSTFLN is this value. FULFLN and the closed form solution (G) for the entire interval are within 2% of each other. This says two things. First, ANSHRT is the correct solution for the numerical integration between the end points. Second, one cannot set up a Newton-Cotes integration scheme over a given interval, and then expect to throw away unwanted sections of the defined interval.

```
      PROGRAM TSTFLN
C
C  THIS PROGRAM USES FILON'S NUMERICAL INTEGRATION
C  METHOD TO FIND THE VALUE OF AN INTEGRAL WITH A
C  SLOWLY OSCILLATING ( COS ( PIZ/3 ) ) TERM AND A
C  RAPIDLY OSCILLATING ( COS ( KZ ) ) TERM INSIDE
C  THE INTEGRAL. ANSHRT IS THE SOLUTION FOR ALL THE
C  POINTS BETWEEN THE END POINTS. FULFLN IS THE FULL
C  FILON SOLUTION ( INCLUDING WEIGHTED END POINTS ).
C  BOTH SOLUTIONS ARE WRITTEN OUT TO A FILE FOR
C  PRINTING.
C
      INTEGER M
      REAL*8 A,B,ZE ZO,COSZ2J,TH,H,BZ,GZ,FZ2J1,COS2J1,
     + SUMBZ,SUMGZ,RSUMBZ,RSUMGZ,AZ,ANSHRT,FZO,COSZO
      REAL*8 FZ2M,COSZ2M,ENDPTS,SINZO,SINZ2M,FULFLN,
     + PI,K,TH2,TH3,TH4,TH5
C
C  OPEN PRINT FILE
C
      OPEN (12,FILE='TSTFLN.PRN',STATUS='UNKNOWN')
C
C  READ IN VARIABLES
C
      PRINT*,' ENTER M = '
      READ*, M
      PRINT*,' ENTER K = '
      READ*, K
C
C  CALCULATE THE CONSTANTS
C
      PI = 4. * ATAN (1.)
      SUMBZ = Ø.
      SUMGZ = Ø.
      A = 1.
      B = -1.
      H = (A - B) / M / 2.
      TH = K * H
      TH2 = TH * TH
      TH3 = TH2 * TH
      TH4 = TH2 * TH2
      TH5 = TH4 * TH
      AZ = (2./45.)*TH3 - (2./315.)*TH5
      BZ = (2./3.) + (2./15.)*TH2 - (4./1Ø5.)*TH4
      GZ = (4./3.) - (2./15.)*TH2 + (1./27Ø.)*TH4
C
C  CALCULATE MIDDLE POINTS
C
      DO 1ØØ J = 1,M
      ZE = B + (2. * H * J)
      ZO = B + ((2. * H * J) - H)
      IF (J .EQ. M) GOTO 5Ø
      FZ2J = COS (PI * ZE / 3.)
```

```
      COSZ2J = COS (K * ZE)
      RSUMBZ = FZ2J * COSZ2J
      SUMBZ = SUMBZ + RSUMBZ
50    FZ2J1 = COS (PI * ZO / 3.)
      COS2J1 = COS (K * ZO)
      RSUMGZ = FZ2J1 * COS2J1
      SUMGZ = SUMGZ + RSUMGZ
100   CONTINUE
C
C  WEIGHT THE MIDDLE POINTS
C
      SUMBZ = SUMBZ * BZ
      SUMGZ = SUMGZ * GZ
      ANSHRT = (SUMBZ + SUMGZ) * H
C
C  CALCULATE THE END POINTS
C
      FZO = COS (PI * B / 3.)
      COSZO = COS (K * B)
      FZ2M = COS (PI * A / 3.)
      COSZ2M = COS (K * A)
      SINZO = SIN (K * B)
      SINZ2M = SIN (K * A)
      ENDPTS = ((AZ*FZ2M*SINZ2M)-(AZ*FZO*SINZO)+
     + ((BZ*FZO*COSZO)/2.)+((BZ*FZ2M*COSZ2M)/2.))*H
      FULFLN = ANSHRT + ENDPTS
C
C  WRITE OUT THE SOLUTIONS TO A FILE
C
      WRITE (12,200)
200   FORMAT (1X,'    M =      ',2X,'SOLUTION    ',
     +2X,'FULL    ')
      WRITE (12,210)
210   FORMAT (15X,'MINUS     ',2X,'  SOLUTION  ')
      WRITE (12,220)
220   FORMAT (15X,'END POINTS  ')
      WRITE (12,225)
225   FORMAT (1X,'')
      WRITE (12,230) M , ANSHRT , FULFLN
230   FORMAT (5X,I4,5X,E12.6,2X,E12.6)
      STOP
      END
```

Appendix C

Programs Used for Evaluations of Numerical Solution (UNIFLD, TRIFLD)

Program UNIFLD was used to test the numerical solution against the far-field and ICF solutions for a dipole antenna with a uniform current density. The program uses function routines for calculation of each of the three solutions -- outputs from the program are:

MAGICF = Vector potential magnitude of ICF solution

MAGFAR = Vector potential magnitude of far-field solution

MAGSUM = Vector potential magnitude of numerical solution

Program TRIFLD was used to test the numerical solution against the other two solutions for the same antenna with a triangular shaped current density. The solution outputs are named the same as those in the UNIFLD program. The function routines in TRIFLD have been changed from those in UNIFLD to solve for the triangle current density.

```
      PROGRAM UNIFLD
C
C  UNIFORM CURRENT DISTRIBUTION ON DIPOLE ANTENNA
C
C  THIS PROGRAM CALCULATES THE VECTOR POTENTIAL BOTH IN
C  COMPLEX NUMBER AND MAGNITUDE FORM BY THREE
C  DIFFERENT METHODS . THE METHODS ARE FAR-FIELD SOLUTION,
C  INCOMPLETE CYLINDRICAL FUNCTIONS (ICF), AND A NUMERICAL
C  SUMMATION SOLUTION. THE VECTOR POTENTIAL IS ALSO
C  CALCULATED AT A VECTOR DISTANCE  (R)   , OVER A RANGE
C  OF ANGLES THETA. THE SOLUTIONS ARE WRITTEN OUT TO A
C  FILE THAT IS FORMATED INTO A TABLE.
C
      REAL*8 PI,Y,Z,K,THETA,H,R,X,I,STRT,FINSH,INC
      REAL*8 MAGFAR,MAGSUM,MAGICF
      COMPLEX J,I1TOP,I1BOT,I1,SUMFLD,FARFLD
      COMPLEX AFDICF,AFDSUM,AFDFAR
      INTEGER M
C
C  OPEN PRINT FILES
C
      OPEN (11,FILE='UNIFLD.PRN',STATUS='UNKNOWN')
C
C  ESTABLISH THE CONSTANTS
C
      J = CMPLX (0.,1.)
      PI = 4. * ATAN (1.)
C
C  READ IN THE VARIABLES
C
      PRINT*,' ENTER R '
      READ*, R
      PRINT*,' ENTER K '
      READ*, K
      PRINT*,' ENTER M '
      READ*, M
      PRINT*,' ENTER START ANGLE '
      READ*, STRT
      PRINT*,' ENTER FINISH ANGLE '
      READ*, FINSH
      PRINT*,' ENTER INCREMENT ANGLE '
      READ*, INC
C
C  CALCULATE THE DELTA WIDTH
C
      H = 1. / M
C
C  ESTABLISH THE FORMAT FOR THE MAGNITUDE FILE
C
      WRITE (11,600)
600   FORMAT (1X,'  -------------------------------------
     +-------------------')
      WRITE (11,610)
```

```
610     FORMAT (1X,' |          |      MAGNITUDE OF VECTOR
     +POTENTIAL                 | ')
        WRITE (11,620)
620     FORMAT (1X,' |          |----------------------------
     +-------------------| ')
        WRITE (11,630)
630     FORMAT (1X,' |          |       UNIFORM CURRENT
     +DISTRIBUTION                 | ')
        WRITE (11,620)
        WRITE (11,635) R , M , K
635     FORMAT (1X,' |          |  R =  ',F5.1,'    |  M =  '
     +,I5,'    |  K =  ',F5.0,'    | ')
        WRITE ( 11, 620)
        WRITE (11,640)
640     FORMAT (1X,' |  THETA   |      FAR-        |      ICF
     +        |  NUMERICAL     | ')
        WRITE (11,650)
650     FORMAT (1X,' |  (DEG)   |      FIELD       |
     +          |                  | ')
        WRITE (11,660)
660     FORMAT (1X,' |--------- ---------------
     +-------------- --------------| ')
C
C   FIND VECTOR POTENTIAL OVER RANGE OF THETAS
C
        DO 200 I = STRT,FINSH,INC
          THETA = I * (PI / 180.)
          Y = SIN (THETA) * R
          Z = COS (THETA) * R
C
C   FIND ICF VALUE
C
          I1TOP = I1 (Y,Z,K,PI,J)
          X = -Z
          I1BOT = I1 (Y,X,K,PI,J)
C
C   ICF SOLUTION IN COMPLEX NUMBER FORM
C
          AFDICF = I1TOP + I1BOT
C
C   NUMERICAL ANSWER IN COMPLEX NUMBER FORM
C
          AFDSUM = SUMFLD(Y,Z,K,M,H)/4./PI * H
C
C   MAGNITUDE OF ICF SOLUTION
C
          MAGICF = SQRT(REAL(AFDICF)*REAL(AFDICF) +
     +    AIMAG(AFDICF) * AIMAG(AFDICF))
C
C   MAGNITUDE OF NUMERICAL SOLUTION
C
          MAGSUM = SQRT(REAL(AFDSUM)*REAL(AFDSUM) +
     +    AIMAG(AFDSUM) * AIMAG(AFDSUM))
```

```
C
C  SET FAR-FIELD ANSWERS TO ZERO IF R IS NOT IN FAR-FIELD
C
                IF (R.LT.2Ø.) THEN
                MAGFAR = Ø.
                GOTO 3ØØ
                END IF
C
C  FAR-FIELD SOLUTION IN COMPLEX NUMBER FORM
C
              AFDFAR = FARFLD (K,PI,R,THETA)
C
C  MAGNITUDE OF FAR-FIELD SOLUTION
C
              MAGFAR = SQRT(REAL(AFDFAR)*REAL(AFDFAR) +
     +      AIMAG(AFDFAR) * AIMAG(AFDFAR))
C
C  WRITE OUT SOLUTIONS FOR CURRENT VALUE IF THETA
C
3ØØ         WRITE (11, 33Ø) I , MAGFAR , MAGICF , MAGSUM
33Ø         FORMAT (1X,' |   ',F5.1,'   |   ',E1Ø.4,'    |   ',
     +E1Ø.4,   '    |   ',E1Ø.4,'    | ')
            WRITE (11,66Ø)
2ØØ         CONTINUE
            STOP
            END
C
C FUNCTION ROUTINE THAT CALCULATES THE ICF SOLUTION
C
            COMPLEX FUNCTION I1 (Y,Z,K,PI,J)
            COMPLEX I1,BR,J
            REAL*8 Y,Z,K,PI,T
            IF((ABS(K*Z).LT.1Ø.).OR.(ABS(K*(Z-.5)).LT.1Ø.))THEN
            GOTO 7ØØ
            END IF
            T = Z -.5
            I1 = (BR (Y,K,T,J) - BR (Y,K,Z,J)) / 4. / PI
             RETURN
7ØØ         PRINT*,' K * Y TOO SMALL '
            RETURN
            END
C
            COMPLEX FUNCTION BR(Y,K,ZE,J)
            COMPLEX BR,J
            REAL*8 K,ZE,Y,R,U
            R = SQRT (Y * Y + ZE * ZE)
            U = -K * ZE
            U = 1. / U
            BR = CMPLX(U-(3.*Y*Y+4.*ZE*ZE)*U*U*U/(ZE*ZE),
     +      -R*U*U/ZE)
            BR = BR * CEXP(CMPLX(Ø.,-K * R ))
            BR = J * BR
            RETURN
```

```
      END
C
C  FUNCTION ROUTINE THAT CALCULATES THE NUMERICAL SOLUTION
C
      COMPLEX FUNCTION SUMFLD (Y,Z,K,M,H)
      COMPLEX A2,A,SUMFLD
      REAL*8 Y,Z,K,H,ZJ,ZABS,R
      INTEGER M
      SUMFLD = CMPLX (Ø.,Ø.)
      DO 4ØØ J = 1,M
      ZJ = -.5 + (H *J) - (.5 * H)
      ZABS = ABS (ZJ)
      R = SQRT (Y * Y + (Z - ZJ) * (Z - ZJ))
      A2 = CEXP (CMPLX (Ø.,-K * R ))
      A = A2 / R
      SUMFLD = SUMFLD + A
4ØØ   CONTINUE
      RETURN
      END
C
C  FUNCTION ROUTINE THAT CALCULATES THE FAR-FIELD SOLUTION
C
      COMPLEX FUNCTION FARFLD (K,PI,R,THETA)
      COMPLEX SI,FARFLD
      REAL*8 K,PI,R,THETA,U,UL2,SINU
      U = -COS (THETA) * ABS (K)
      UL2 = U / 2.
      SI = CEXP( CMPLX( Ø.,-K*R)) / 2. / PI / R
      SINU = SIN (UL2)
      FARFLD = SI * SINU / U
      RETURN
      END
```

```
      PROGRAM TRIFLD
C
C  TRIANGULAR CURRENT DISTRIBUTION ON DIPOLE ANTENNA
C
C  THIS PROGRAM CALCULATES THE VECTOR POTENTIAL BOTH IN
C  COMPLEX NUMBER AND MAGNITUDE/PHASE FORM BY THREE
C  DIFFERENT METHODS . THE METHODS ARE FAR-FIELD SOLUTION,
C  INCOMPLETE CYLINDRICAL FUNCTIONS (ICF), AND A NUMERICAL
C  SUMMATION SOLUTION. THE VECTOR POTENTIAL IS ALSO
C  CALCULATED AT A VECTOR DISTANCE  (R)  , OVER A RANGE
C  OF ANGLES THETA. THE SOLUTIONS ARE WRITTEN OUT TO
C  FILES THAT ARE FORMATED INTO A TABLE.
C
      REAL*8 PI,Y,Z,K,THETA,H,R,X,I,STRT,FINSH,INC,MAGICF
      REAL*8 MAGFAR,PASFAR,MAGSUM,PASSUM,PASICF
      COMPLEX J,I1TOP,I1BOT,I1BOTH,I1,I2TOP,I2BOT,I2BOTH
      COMPLEX AFDICF,AFDSUM,AFDFAR,SUMFLD,FARFLD,I2,A1,A2
      INTEGER M
C
C  OPEN PRINT FILES
C
      OPEN (9,FILE='MTRIFLD.PRN',STATUS='UNKNOWN')
      OPEN (10,FILE='PTRIFLD.PRN',STATUS='UNKNOWN')
C
C  ESTABLISH THE CONSTANTS
C
      J = CMPLX (0.,1.)
      PI = 4. * ATAN (1.)
C
C  READ IN THE VARIABLES
C
      PRINT*,' ENTER R '
      READ*, R
      PRINT*,' ENTER K '
      READ*, K
      PRINT*,' ENTER M '
      READ*, M
      PRINT*,' ENTER START ANGLE '
      READ*, STRT
      PRINT*,' ENTER FINISH ANGLE '
      READ*, FINSH
      PRINT*,' ENTER INCREMENT ANGLE '
      READ*, INC
C
C  CALCULATE THE DELTA WIDTH
C
      H = 1. / M
C
C  ESTABLISH THE FORMAT FOR THE MAGNITUDE FILE
C
      WRITE (9,600)
600   FORMAT (1X,' ------------------------------------
     +-------------------')
```

```
      WRITE (9,610)
610   FORMAT (1X,' |             |      MAGNITUDE OF VECTOR
     +POTENTIAL                 | ')
615   FORMAT (1X,' |             |      PHASE OF VECTOR
     +POTENTIAL                 | ')
      WRITE (9,620)
620   FORMAT (1X,' |             |-----------------------------
     +--------------------| ')
      WRITE (9,630)
630   FORMAT (1X,' |             |    TRIANGULAR CURRENT
     +DISTRIBUTION              | ')
      WRITE (9,620)
      WRITE (9,635) R , M , K
635   FORMAT (1X,' |             |  R =  ',F5.1,'    |  M =  '
     +,I5,'    |  K =  ',F5.0,'    | ')
      WRITE ( 9, 620)
      WRITE (9,640)
640   FORMAT (1X,' |  THETA  |      FAR-       |      ICF
     +        |  NUMERICAL     | ')
      WRITE (9,650)
650   FORMAT (1X,' |  (DEG)  |      FIELD      |
     +        |                | ')
      WRITE (9,660)
660   FORMAT (1X,' |--------- ---------------
     +-------------- ---------------|')
C
C  ESTABLISH THE FORMAT OF THE PHASE FILE
C
      WRITE (10,600)
      WRITE (10,615)
      WRITE (10,620)
      WRITE (10,630)
      WRITE (10,620)
      WRITE (10,635) R , M , K
      WRITE (10,620)
      WRITE (10,640)
      WRITE (10,650)
      WRITE (10,660)
C
C  FIND VECTOR POTENTIAL OVER RANGE OF THETAS
C
      DO 200 I = STRT,FINSH,INC
        THETA = I * (PI / 180.)
        Y = SIN (THETA) * R
        Z = COS (THETA) * R
C
C  FIND ICF VALUE
C
        I1TOP = I1 (Y,Z,K,PI,J,I2,A1,A2)
        I2TOP = I2
        X = -Z
        I1BOT = I1 (Y,X,K,PI,J,I2,A1,A2)
        I2BOT = I2
```

```
      I1BOTH = I1TOP + I1BOT
      I2BOTH = (I2TOP + I2BOT) * (-2.)
C
C  ICF SOLUTION IN COMPLEX NUMBER FORM
C
      AFDICF = I1BOTH + I2BOTH
C
C  NUMERICAL ANSWER IN COMPLEX NUMBER FORM
C
      AFDSUM = SUMFLD(Y,Z,K,M,H)/4./PI * H
C
C  MAGNITUDE OF ICF SOLUTION
C
      MAGICF = SQRT(REAL(AFDICF)*REAL(AFDICF) +
     +   AIMAG(AFDICF) * AIMAG(AFDICF))
C
C  PHASE OF ICF SOLUTION
C
      PASICF = ATAN2(AIMAG(AFDICF),REAL(AFDICF))
     +    / PI * 180.
C
C  MAGNITUDE OF NUMERICAL SOLUTION
C
      MAGSUM = SQRT(REAL(AFDSUM)*REAL(AFDSUM) +
     +   AIMAG(AFDSUM) * AIMAG(AFDSUM))
C
C  PHASE OF NUMERICAL SOLUTION
C
      PASSUM = ATAN2(AIMAG(AFDSUM),REAL(AFDSUM))
     +    / PI * 180.
C
C  SET FAR-FIELD ANSWERS TO ZERO IF R IS NOT IN FAR-FIELD
C
        IF (R.LT.20.) THEN
        MAGFAR = 0.
        PASFAR = 0.
        GOTO 300
        END IF
C
C  FAR-FIELD SOLUTION IN COMPLEX NUMBER FORM
C
      AFDFAR = FARFLD (K,PI,R,THETA)
C
C  MAGNITUDE OF FAR-FIELD SOLUTION
C
      MAGFAR = SQRT(REAL(AFDFAR)*REAL(AFDFAR) +
     +   AIMAG(AFDFAR) * AIMAG(AFDFAR))
C
C  PHASE OF FAR-FIELD SOLUTION
C
      PASFAR = ATAN2(AIMAG(AFDFAR),REAL(AFDFAR))
     +    / PI * 180.
C
```

```
C  WRITE OUT SOLUTIONS FOR CURRENT VALUE OF THETA
C
300     WRITE (9, 330) I , MAGFAR , MAGICF , MAGSUM
        WRITE (10,330) I , PASFAR , PASICF , PASSUM
330     FORMAT (1X,' |  ',F5.1,'  |  ',E10.4,'   |  ',
     +E10.4,  '   |  ',E10.4,'   | ')
        WRITE (9,660)
        WRITE (10,660)
200     CONTINUE
        STOP
        END
C
C FUNCTION ROUTINE THAT CALCULATES THE ICF SOLUTION
C
        COMPLEX FUNCTION I1 (Y,Z,K,PI,J,I2,A1,A2)
        COMPLEX I1,BR,J,I2,A1,A2
        REAL*8 Y,Z,K,PI,T
        IF((ABS(K*Z).LT.10.).OR.(ABS(K*(Z-.5)).LT.10.))THEN
        GOTO 700
        END IF
        T = Z -.5
        I1 = (BR (Y,K,T,J) - BR (Y,K,Z,J)) / 4. / PI
        A1 =CEXP(CMPLX(0.,-K*SQRT(Y*Y+(Z-.5)*(Z-.5))))
        A2 = CEXP (CMPLX (0., -K * SQRT(Y * Y + Z * Z )))
        I2 = (A1 - A2) / 4. / PI / ABS(K) * J
        I2 = I2 + (Z * I1)
         RETURN
700     PRINT*,' K * Y TOO SMALL '
        RETURN
        END
C
        COMPLEX FUNCTION BR(Y,K,ZE,J)
        COMPLEX BR,J
        REAL*8 K,ZE,Y,R,U
        R = SQRT (Y * Y + ZE * ZE)
        U = -K * ZE
        U = 1. / U
        BR = CMPLX(U-(3.*Y*Y+4.*ZE*ZE)*U*U*U/(ZE*ZE),
     +  -R*U*U/ZE)
        BR = BR * CEXP(CMPLX(0.,-K * R ))
        BR = J * BR
        RETURN
        END
C
C  FUNCTION ROUTINE THAT CALCULATES THE NUMERICAL SOLUTION
C
        COMPLEX FUNCTION SUMFLD (Y,Z,K,M,H)
        COMPLEX A2,A,SUMFLD
        REAL*8 Y,Z,K,H,ZJ,ZABS,A1,R
        INTEGER M
        SUMFLD = CMPLX (0.,0.)
        DO 400 J = 1,M
        ZJ = -.5 + (H *J) - (.5 * H)
```

```
      ZABS = ABS (ZJ)
      A1 = 1. - (2. * ZABS)
      R = SQRT (Y * Y + (Z - ZJ) * (Z - ZJ))
      A2 = CEXP (CMPLX (Ø.,-K * R ))
      A = A1 * A2 / R
      SUMFLD = SUMFLD + A
400   CONTINUE
      RETURN
      END
C
C  FUNCTION ROUTINE THAT CALCULATES THE FAR-FIELD SOLUTION
C
      COMPLEX FUNCTION FARFLD (K,PI,R,THETA)
      COMPLEX A1,A2,FARFLD
      REAL*8 K,PI,R,THETA,U,U4
      A1 = CEXP (CMPLX (Ø.,-K * R ))
      U = -COS (THETA) * ABS (K)
      U4 = U / 4.
      A2 = ( SIN (U4) / U4 ) * ( SIN (U4) / U4 ) * .5
      FARFLD = A1 / 4. / PI / R * A2
      RETURN
      END
```

Appendix D

Exact Solutions for Radiation from Rectangular and Triangular Current Distributions on Dipoles

by

David A. Lee

USAF Institute of Technology

Wright-Patterson AFB, Ohio 45433

INTRODUCTION

Radiation from the rectangular current distribution of Figure 9 is often studied as a useful approximation to radiation from a short dipole, and radiation from the triangular distribution of Figure 8 is often studied as a useful approximation to radiation from a dipole of intermediate length (2:106). In standard works like references (2;3), the fields produced by these distributions are treated approximately. It is of course desirable to have exact solutions whenever these can be conveniently obtained. While exact solutions for other distributions which are useful for modeling current distributions in actual dipoles are known--for example, the exact solution for radiation from a piecewise-sinusoidal distribution as given in reference (2)--it is nevertheless useful to have other exact solutions for such purposes as the evaluation of numerical methods for solving radiation problems. This note shows that radiation from both the current distributions shown in Figures 8 and 9 can be expressed exactly in terms of known special functions, specifically, incomplete cylindrical functions (22). Series and asymptotic expansions are available for these functions, which may be used in radiation problems. We give an example of such an application, in the assessment of a numerical scheme.

TWO EXACT SOLUTIONS

Consider first radiation from the current distribution of Figure 9. The vector potential for this case is

$$A(\bar{r}) = \underline{k}\, J\, I_1(r,z) \tag{66}$$

where the function $I_1(r,z)$ is given by

$$I_1(r,z) \equiv \int_{-L/2}^{L/2} \frac{e^{jk|r^2+(z-u)^2|^{1/2}}}{|r^2+(z-u)^2|^{1/2}}\, du \tag{67}$$

Set v = z - u, so that

$$I_1(r,z) = \int_{z-L/2}^{z+L/2} \frac{e^{jk|r^2+v^2|^{1/2}}}{|r^2+v^2|^{1/2}}\, dv \tag{68}$$

We treat first the case r = Ø. Set v = ry, to find

$$I_1 = \int_{\frac{z-L/2}{r}}^{\frac{z+L/2}{r}} \frac{e^{jk|1+y^2|^{1/2}}}{|1+y^2|^{1/2}}\, dy \tag{69}$$

Since the problem is symmetric about $z = 0$ we may consider only $z > 0$ without loss of generality. We'll consider separately the cases $z > d/2$ and $z < d/2$. If $z > d/2$, then y is positive over the entire interval of integration in (69). Then we may set

$$t^2 = 1 + Y^2, \quad t = |1 + Y^2|^{1/2}, \quad Y = |t^2 - 1|^{1/2} \tag{70}$$

and write

$$I_1 = \int_{t_1}^{t_2} \frac{e^{jkrt}}{|t^2 - 1|^{1/2}} dt \tag{71}$$

where

$$t_1 = \left| 1 + \left(\frac{z - L/2}{r}\right)^2 \right|^{1/2}, \quad t_2 = \left| 1 + \left(\frac{z + L/2}{r}\right)^2 \right|^{1/2}$$

In reference (22), Agrest and Maksimov study several members of the class of functions called incomplete cylindrical functions. In particular, they consider incomplete Hankel functions $H_\nu(\beta, z)$ defined by:

$$H^1_\nu(\beta, z) \equiv \frac{-2i\, e^{-i\nu\pi} z^\nu}{F_\nu} \int_1^{\cosh\beta} e^{iz\tau} (\tau^2 - 1)^{\nu - 1/2} \tag{72}$$

for $\beta > 0$ and $\mathrm{Re}(\nu + 1/2) > 0$, where

$$A_\nu \equiv 2^\nu \, \Gamma(\nu + 1/2)\, \Gamma(1/2)$$

Thus for the case at hand (i.e. $z > d/2$, $r > 0$),

$$I_1 = \frac{\pi i}{2}\left[H_0(\cosh^{-1} t_{2}, kr) - H_0(\cos^{-1} t_1, kr)\right] \tag{73}$$

since $A_0 = \Gamma^2(1/2) = \pi$.

Series and asymptotic expansions given in Sections 7 and 9, respectively, of reference (22) permit the numerical evaluation of the incomplete Hankel functions of (73).

Turning now to the case $z < d/2$, we see that (69) may then be written in the form

$$I_1 = \int_{\frac{-L/2+z}{r}}^{0} \frac{e^{ikr|1+Y^2|^{1/2}}}{|1+Y^2|^{1/2}}\,dY + \int_0^{\frac{L/2+z}{r}} \frac{e^{ikr|1+Y^2|^{1/2}}}{|1+Y^2|^{1/2}}\,dY$$

$$= \int_0^{\frac{L/2-z}{r}} \frac{e^{ikr|1+Y^2|^{1/2}}}{|1+Y^2|^{1/2}}\,dY + \int_0^{\frac{L/2+z}{r}} \frac{e^{ikr|1+Y^2|^{1/2}}}{|1+Y^2|^{1/2}}\,dY \tag{74}$$

Now the variables of integration are positive on the intervals of integration of both the integrals in (74). We may apply the same change of integration variable that took us from (67) to (71), to each integral in (74). Then (72) allows us to write

$$I_1 = \frac{\pi i}{2}\left[\mathcal{H}_0(\cosh^{-1} t_1, kr) + \mathcal{H}_0(\cosh^{-1} t_2, kr)\right] \tag{75}$$

It follows from (74) and these last consideration (or also directly from (75) that, when z = d/2,

$$I_1 = \frac{\pi i}{2}\left[\mathcal{H}_0(\cosh^{-1} t_2, kr)\right] \tag{76}$$

Equations (73), (75) and (76) give exact expressions for the vector potential of the radiation resulting from the current distribution of Figure 9, for all z and all r > Ø. To deal with the case r = Ø, note that

$$\begin{aligned} I_1(0,z) &\equiv \int_{-L/2}^{L/2} \frac{e^{ik|(z-u)^2|^{1/2}}}{|(z-u)^2|^{1/2}}\,du \\ &= \int_{-L/2}^{L/2} \frac{e^{ik|z-u|}}{|z-u|}\,du \end{aligned} \tag{77}$$

For r = Ø, the observation point is inside the radiator if z < d/2, and we ignore this (not physical) case. For r = Ø and z > d/2, we have

$$I_1(0,z) = \int_{-L/2}^{L/2} \frac{e^{ik(z-u)}}{(z-u)}\, du \tag{78}$$

or, setting v = z - u,

$$I_1(0,z) = \int_{z-L/2}^{z+L/2} \frac{e^{ikv}}{v}\, dv$$

$$= \bar{E}_1\left[i\,(z - L/2)\right] - \bar{E}_1\left[i\,(z + L/2)\right] \tag{79}$$

where $E_1(w)$ denotes the exponential integral and $\bar{\ }$ denotes complex conjugate.

Series and asymptotic expansions useful for evaluating the exponential integral are found in Chapter 5 of reference (32).

Now let us consider the current distribution of Figure 8. For this case,

$$F = k\,C\,I_2 \; \text{[illegible]} \tag{80}$$

where

$$I_2(r,z) \equiv \int_{-L/2}^{L/2} \left(1 - \frac{2|u|}{L}\right) \frac{e^{ik|r^2+(z-u)^2|^{1/2}}}{|r^2+(z-u)^2|^{1/2}}\, du \tag{81}$$

$$= I_1 - \frac{2}{L} I_3(r,z) \tag{82}$$

in which

$$I_3(r,z) = \int_{-L/2}^{L/2} |u| \frac{e^{ik|r^2+(z-u)^2|^{1/2}}}{|r^2+(z-u)^2|^{1/2}}\, du \tag{83}$$

$$= \int_0^{L/2} Y \frac{e^{ik|r^2+(z+Y)^2|^{1/2}}}{|r^2+(z+Y)^2|^{1/2}}\, dY + \int_0^{L/2} u \frac{e^{ik|r^2+(z-u)^2|^{1/2}}}{|r^2+(z-u)^2|^{1/2}}\, du \tag{84}$$

Straightforward additions and subtractions show that

$$I_3 = \int_0^{L/2} (z+Y) \frac{e^{ik|r^2+(z+Y)^2|^{1/2}}}{|r^2+(z+Y)^2|^{1/2}}\, d(z+Y) - z \int_0^{L/2} \frac{e^{ik|r^2+(z+Y)^2|^{1/2}}}{|r^2+(z+Y)^2|^{1/2}}\, dY$$

$$- \int_0^{L/2} (z-u) \frac{e^{ik|r^2+(z-u)^2|^{1/2}}}{|r^2+(z-u)^2|^{1/2}}\, d(z-u) + z \int_0^{L/2} \frac{e^{ik|r^2+(z-u)^2|^{1/2}}}{|r^2+(z-u)^2|^{1/2}}\, du \tag{85}$$

Now, the first and third integrals of (85) are integrals of exact differentials, while the second and fourth integrals can be evaluated in terms of incomplete Hankel functions by arguments similar to those given above to evaluate $I_1(r,z)$. Carrying out straightforward but tedious manipulations, one finds

$$I_3(r,z) = -\frac{i}{k}\left(e^{ikrt_1} - 2e^{ikrt_3} + e^{ikrt_2}\right) + \tag{86}$$

$$+ z\left[\mathcal{H}_0(\cosh^{-1} t_1, kr) - 2\mathcal{H}_0(\cosh^{-1} t_3, kr) + \mathcal{H}_0(\cosh^{-1} t_2, kr)\right]$$

when $z > d/2$, where $t_3 \equiv \sqrt{1 + z^2/r^2}$, and

$$I_3(r,z) = -\frac{i}{k}\left(e^{ikrt_1} - 2e^{ikrt_2} + e^{ikrt_2}\right) \tag{87}$$

$$+ z\left[\mathcal{H}_0(\cosh^{-1} t_1, kr) + \mathcal{H}_0(\cosh^{-1} t_2, kr)\right]$$

when $z < d/2$. Equations (86) and (87) give exact expressions for the vector potential of radiation from the system of Figure 8 for all positive z and all $r > 0$. For $r = 0$ and $z > d/2$, we find

$$I_3 = -\frac{2i}{k} e^{ikz} \left(\cosh kL/2 - 1 \right)$$

$$- z\left[\bar{E}_1 \left(i \left(L/2 + z \right) \right) + \bar{E}_1 \left(i \left(z - L/2 \right) \right) \right] \tag{88}$$

Equation (88) completes the determination of the vector potential for radiation from the system of Figure 8. Of course, it is the fields rather than the vector potential which one wishes to know. Expressions given in reference (22) permit one to evaluate the derivatives of the vector potential which give the fields.

Appendix E

Solution Comparison Tables

The following tables show the results of comparisons made of both the uniform and triangular current distributions, for various values of $\bar{r}$ and M.

Table II

	MAGNITUDE OF VECTOR POTENTIAL		
	UNIFORM CURRENT DISTRIBUTION		
	R = 5.Ø	M = 5Ø	K = 63.
THETA (DEG)	FAR-FIELD	ICF	NUMERICAL
15.Ø	Ø.ØØØØE+ØØ	Ø.4457E-Ø3	Ø.4743E-Ø3
18.Ø	Ø.ØØØØE+ØØ	Ø.5346E-Ø3	Ø.5678E-Ø3
21.Ø	Ø.ØØØØE+ØØ	Ø.4922E-Ø3	Ø.5216E-Ø3
24.Ø	Ø.ØØØØE+ØØ	Ø.2636E-Ø3	Ø.2784E-Ø3
27.Ø	Ø.ØØØØE+ØØ	Ø.1483E-Ø3	Ø.1557E-Ø3
3Ø.Ø	Ø.ØØØØE+ØØ	Ø.5Ø76E-Ø3	Ø.5332E-Ø3
33.Ø	Ø.ØØØØE+ØØ	Ø.5797E-Ø3	Ø.6Ø71E-Ø3
36.Ø	Ø.ØØØØE+ØØ	Ø.2Ø62E-Ø3	Ø.2143E-Ø3
39.Ø	Ø.ØØØØE+ØØ	Ø.43Ø9E-Ø3	Ø.4479E-Ø3
42.Ø	Ø.ØØØØE+ØØ	Ø.6782E-Ø3	Ø.7Ø3ØE-Ø3
45.Ø	Ø.ØØØØE+ØØ	Ø.1932E-Ø3	Ø.1978E-Ø3
48.Ø	Ø.ØØØØE+ØØ	Ø.64Ø3E-Ø3	Ø.6589E-Ø3
51.Ø	Ø.ØØØØE+ØØ	Ø.6582E-Ø3	Ø.6748E-Ø3
54.Ø	Ø.ØØØØE+ØØ	Ø.3656E-Ø3	Ø.3722E-Ø3
57.Ø	Ø.ØØØØE+ØØ	Ø.9448E-Ø3	Ø.9626E-Ø3
6Ø.Ø	Ø.ØØØØE+ØØ	Ø.21Ø4E-Ø3	Ø.2Ø87E-Ø3
63.Ø	Ø.ØØØØE+ØØ	Ø.1161E-Ø2	Ø.1176E-Ø2
66.Ø	Ø.ØØØØE+ØØ	Ø.413ØE-Ø3	Ø.413ØE-Ø3
69.Ø	Ø.ØØØØE+ØØ	Ø.1476E-Ø2	Ø.1488E-Ø2

Table III

THETA (DEG)	MAGNITUDE OF VECTOR POTENTIAL — UNIFORM CURRENT DISTRIBUTION — R = 5.Ø	M = 5ØØ	K = 63.
	FAR-FIELD	ICF	NUMERICAL
15.Ø	Ø.ØØØØE+ØØ	Ø.4457E-Ø3	Ø.4459E-Ø3
18.Ø	Ø.ØØØØE+ØØ	Ø.5346E-Ø3	Ø.5349E-Ø3
21.Ø	Ø.ØØØØE+ØØ	Ø.4922E-Ø3	Ø.4925E-Ø3
24.Ø	Ø.ØØØØE+ØØ	Ø.2636E-Ø3	Ø.2637E-Ø3
27.Ø	Ø.ØØØØE+ØØ	Ø.1483E-Ø3	Ø.1483E-Ø3
3Ø.Ø	Ø.ØØØØE+ØØ	Ø.5Ø76E-Ø3	Ø.5Ø78E-Ø3
33.Ø	Ø.ØØØØE+ØØ	Ø.5797E-Ø3	Ø.58ØØE-Ø3
36.Ø	Ø.ØØØØE+ØØ	Ø.2Ø62E-Ø3	Ø.2Ø63E-Ø3
39.Ø	Ø.ØØØØE+ØØ	Ø.43Ø9E-Ø3	Ø.4311E-Ø3
42.Ø	Ø.ØØØØE+ØØ	Ø.6782E-Ø3	Ø.6785E-Ø3
45.Ø	Ø.ØØØØE+ØØ	Ø.1932E-Ø3	Ø.1932E-Ø3
48.Ø	Ø.ØØØØE+ØØ	Ø.64Ø3E-Ø3	Ø.64Ø5E-Ø3
51.Ø	Ø.ØØØØE+ØØ	Ø.6582E-Ø3	Ø.6584E-Ø3
54.Ø	Ø.ØØØØE+ØØ	Ø.3656E-Ø3	Ø.3657E-Ø3
57.Ø	Ø.ØØØØE+ØØ	Ø.9448E-Ø3	Ø.945ØE-Ø3
6Ø.Ø	Ø.ØØØØE+ØØ	Ø.21Ø4E-Ø3	Ø.21Ø4E-Ø3
63.Ø	Ø.ØØØØE+ØØ	Ø.1161E-Ø2	Ø.1162E-Ø2
66.Ø	Ø.ØØØØE+ØØ	Ø.413ØE-Ø3	Ø.413ØE-Ø3
69.Ø	Ø.ØØØØE+ØØ	Ø.1476E-Ø2	Ø.1477E-Ø2

Table IV

	MAGNITUDE OF VECTOR POTENTIAL		
	UNIFORM CURRENT DISTRIBUTION		
	R = 25.0	M = 50	K = 63.
THETA (DEG)	FAR-FIELD	ICF	NUMERICAL
15.0	0.8742E-04	0.8749E-04	0.9311E-04
18.0	0.1056E-03	0.1056E-03	0.1122E-03
21.0	0.9805E-04	0.9807E-04	0.1040E-03
24.0	0.5326E-04	0.5324E-04	0.5631E-04
27.0	0.2338E-04	0.2365E-04	0.2494E-04
30.0	0.9784E-04	0.9799E-04	0.1030E-03
33.0	0.1156E-03	0.1156E-03	0.1212E-03
36.0	0.4298E-04	0.4291E-04	0.4481E-04
39.0	0.7896E-04	0.7926E-04	0.8252E-04
42.0	0.1344E-03	0.1344E-03	0.1395E-03
45.0	0.3987E-04	0.3979E-04	0.4112E-04
48.0	0.1196E-03	0.1199E-03	0.1235E-03
51.0	0.1328E-03	0.1328E-03	0.1363E-03
54.0	0.5641E-04	0.5712E-04	0.5845E-04
57.0	0.1841E-03	0.1843E-03	0.1880E-03
60.0	0.8493E-05	0.1142E-04	0.1147E-04
63.0	0.2196E-03	0.2201E-03	0.2232E-03
66.0	0.6046E-04	0.6135E-04	0.6198E-04
69.0	0.2700E-03	0.2709E-03	0.2732E-03

Table V

THETA (DEG)	MAGNITUDE OF VECTOR POTENTIAL		
	UNIFORM CURRENT DISTRIBUTION		
	R = 25.0	M = 500	K = 63.
	FAR-FIELD	ICF	NUMERICAL
15.0	0.8742E-04	0.8749E-04	0.8754E-04
18.0	0.1056E-03	0.1056E-03	0.1057E-03
21.0	0.9805E-04	0.9807E-04	0.9813E-04
24.0	0.5326E-04	0.5324E-04	0.5326E-04
27.0	0.2338E-04	0.2365E-04	0.2366E-04
30.0	0.9784E-04	0.9799E-04	0.9804E-04
33.0	0.1156E-03	0.1156E-03	0.1157E-03
36.0	0.4298E-04	0.4291E-04	0.4293E-04
39.0	0.7896E-04	0.7926E-04	0.7929E-04
42.0	0.1344E-03	0.1344E-03	0.1345E-03
45.0	0.3987E-04	0.3979E-04	0.3980E-04
48.0	0.1196E-03	0.1199E-03	0.1199E-03
51.0	0.1328E-03	0.1328E-03	0.1328E-03
54.0	0.5641E-04	0.5712E-04	0.5714E-04
57.0	0.1841E-03	0.1843E-03	0.1844E-03
60.0	0.8493E-05	0.1142E-04	0.1143E-04
63.0	0.2196E-03	0.2201E-03	0.2201E-03
66.0	0.6046E-04	0.6135E-04	0.6134E-04
69.0	0.2700E-03	0.2709E-03	0.2710E-03

Table VI

	MAGNITUDE OF VECTOR POTENTIAL		
	UNIFORM CURRENT DISTRIBUTION		
	R = 5Ø.Ø	M = 5Ø	K = 63.
THETA (DEG)	FAR-FIELD	ICF	NUMERICAL
15.Ø	Ø.4371E-Ø4	Ø.4372E-Ø4	Ø.4656E-Ø4
18.Ø	Ø.5279E-Ø4	Ø.5279E-Ø4	Ø.56Ø9E-Ø4
21.Ø	Ø.49Ø3E-Ø4	Ø.49Ø3E-Ø4	Ø.5197E-Ø4
24.Ø	Ø.2663E-Ø4	Ø.2663E-Ø4	Ø.2813E-Ø4
27.Ø	Ø.1169E-Ø4	Ø.1172E-Ø4	Ø.1237E-Ø4
3Ø.Ø	Ø.4892E-Ø4	Ø.4894E-Ø4	Ø.5145E-Ø4
33.Ø	Ø.5781E-Ø4	Ø.5781E-Ø4	Ø.6Ø6ØE-Ø4
36.Ø	Ø.2149E-Ø4	Ø.2148E-Ø4	Ø.2243E-Ø4
39.Ø	Ø.3948E-Ø4	Ø.3952E-Ø4	Ø.4114E-Ø4
42.Ø	Ø.672ØE-Ø4	Ø.672ØE-Ø4	Ø.6974E-Ø4
45.Ø	Ø.1993E-Ø4	Ø.1992E-Ø4	Ø.2Ø59E-Ø4
48.Ø	Ø.5978E-Ø4	Ø.5982E-Ø4	Ø.6165E-Ø4
51.Ø	Ø.6641E-Ø4	Ø.664ØE-Ø4	Ø.682ØE-Ø4
54.Ø	Ø.2821E-Ø4	Ø.2829E-Ø4	Ø.2895E-Ø4
57.Ø	Ø.92Ø7E-Ø4	Ø.921ØE-Ø4	Ø.9394E-Ø4
6Ø.Ø	Ø.4247E-Ø5	Ø.4653E-Ø5	Ø.4721E-Ø5
63.Ø	Ø.1Ø98E-Ø3	Ø.1Ø99E-Ø3	Ø.1114E-Ø3
66.Ø	Ø.3Ø23E-Ø4	Ø.3Ø34E-Ø4	Ø.3Ø67E-Ø4
69.Ø	Ø.135ØE-Ø3	Ø.1351E-Ø3	Ø.1362E-Ø3

Table VII

THETA (DEG)	MAGNITUDE OF VECTOR POTENTIAL		
	UNIFORM CURRENT DISTRIBUTION		
	R = 50.0	M = 500	K = 63.
	FAR-FIELD	ICF	NUMERICAL
15.0	0.4371E-04	0.4372E-04	0.4374E-04
18.0	0.5279E-04	0.5279E-04	0.5282E-04
21.0	0.4903E-04	0.4903E-04	0.4906E-04
24.0	0.2663E-04	0.2663E-04	0.2664E-04
27.0	0.1169E-04	0.1172E-04	0.1173E-04
30.0	0.4892E-04	0.4894E-04	0.4897E-04
33.0	0.5781E-04	0.5781E-04	0.5784E-04
36.0	0.2149E-04	0.2148E-04	0.2149E-04
39.0	0.3948E-04	0.3952E-04	0.3954E-04
42.0	0.6720E-04	0.6720E-04	0.6723E-04
45.0	0.1993E-04	0.1992E-04	0.1993E-04
48.0	0.5978E-04	0.5982E-04	0.5984E-04
51.0	0.6641E-04	0.6640E-04	0.6641E-04
54.0	0.2821E-04	0.2829E-04	0.2830E-04
57.0	0.9207E-04	0.9210E-04	0.9211E-04
60.0	0.4247E-05	0.4653E-05	0.4654E-05
63.0	0.1098E-03	0.1099E-03	0.1099E-03
66.0	0.3023E-04	0.3034E-04	0.3035E-04
69.0	0.1350E-03	0.1351E-03	0.1351E-03

Table VIII

THETA (DEG)	MAGNITUDE OF VECTOR POTENTIAL — TRIANGULAR CURRENT DISTRIBUTION — R = 5.Ø	M = 5Ø	K = 63.
	FAR-FIELD	ICF	NUMERICAL
15.Ø	Ø.ØØØØE+ØØ	Ø.8399E-Ø5	Ø.7817E-Ø5
18.Ø	Ø.ØØØØE+ØØ	Ø.1643E-Ø4	Ø.1533E-Ø4
21.Ø	Ø.ØØØØE+ØØ	Ø.2686E-Ø4	Ø.2512E-Ø4
24.Ø	Ø.ØØØØE+ØØ	Ø.3642E-Ø4	Ø.3418E-Ø4
27.Ø	Ø.ØØØØE+ØØ	Ø.396ØE-Ø4	Ø.3728E-Ø4
3Ø.Ø	Ø.ØØØØE+ØØ	Ø.3154E-Ø4	Ø.2978E-Ø4
33.Ø	Ø.ØØØØE+ØØ	Ø.1466E-Ø4	Ø.1383E-Ø4
36.Ø	Ø.ØØØØE+ØØ	Ø.1187E-Ø4	Ø.113ØE-Ø4
39.Ø	Ø.ØØØØE+ØØ	Ø.1874E-Ø4	Ø.18Ø2E-Ø4
42.Ø	Ø.ØØØØE+ØØ	Ø.3737E-Ø4	Ø.3598E-Ø4
45.Ø	Ø.ØØØØE+ØØ	Ø.6Ø36E-Ø4	Ø.5824E-Ø4
48.Ø	Ø.ØØØØE+ØØ	Ø.4889E-Ø4	Ø.4728E-Ø4
51.Ø	Ø.ØØØØE+ØØ	Ø.2449E-Ø4	Ø.2363E-Ø4
54.Ø	Ø.ØØØØE+ØØ	Ø.5Ø28E-Ø4	Ø.4913E-Ø4
57.Ø	Ø.ØØØØE+ØØ	Ø.746ØE-Ø4	Ø.7319E-Ø4
6Ø.Ø	Ø.ØØØØE+ØØ	Ø.1128E-Ø3	Ø.11Ø6E-Ø3
63.Ø	Ø.ØØØØE+ØØ	Ø.5399E-Ø4	Ø.5294E-Ø4
66.Ø	Ø.ØØØØE+ØØ	Ø.1198E-Ø3	Ø.1177E-Ø3
69.Ø	Ø.ØØØØE+ØØ	Ø.1977E-Ø3	Ø.1924E-Ø3

Table IX

	MAGNITUDE OF VECTOR POTENTIAL		
	TRIANGULAR CURRENT DISTRIBUTION		
	R = 5.Ø	M = 1ØØ	K = 63.
THETA (DEG)	FAR-FIELD	ICF	NUMERICAL
15.Ø	Ø.ØØØØE+ØØ	Ø.8399E-Ø5	Ø.8267E-Ø5
18.Ø	Ø.ØØØØE+ØØ	Ø.1643E-Ø4	Ø.1619E-Ø4
21.Ø	Ø.ØØØØE+ØØ	Ø.2686E-Ø4	Ø.2646E-Ø4
24.Ø	Ø.ØØØØE+ØØ	Ø.3642E-Ø4	Ø.3591E-Ø4
27.Ø	Ø.ØØØØE+ØØ	Ø.396ØE-Ø4	Ø.39Ø5E-Ø4
3Ø.Ø	Ø.ØØØØE+ØØ	Ø.3154E-Ø4	Ø.3112E-Ø4
33.Ø	Ø.ØØØØE+ØØ	Ø.1466E-Ø4	Ø.1447E-Ø4
36.Ø	Ø.ØØØØE+ØØ	Ø.1187E-Ø4	Ø.1175E-Ø4
39.Ø	Ø.ØØØØE+ØØ	Ø.1874E-Ø4	Ø.1855E-Ø4
42.Ø	Ø.ØØØØE+ØØ	Ø.3737E-Ø4	Ø.37Ø4E-Ø4
45.Ø	Ø.ØØØØE+ØØ	Ø.6Ø36E-Ø4	Ø.5982E-Ø4
48.Ø	Ø.ØØØØE+ØØ	Ø.4889E-Ø4	Ø.4847E-Ø4
51.Ø	Ø.ØØØØE+ØØ	Ø.2449E-Ø4	Ø.2429E-Ø4
54.Ø	Ø.ØØØØE+ØØ	Ø.5Ø28E-Ø4	Ø.4994E-Ø4
57.Ø	Ø.ØØØØE+ØØ	Ø.746ØE-Ø4	Ø.7411E-Ø4
6Ø.Ø	Ø.ØØØØE+ØØ	Ø.1128E-Ø3	Ø.112ØE-Ø3
63.Ø	Ø.ØØØØE+ØØ	Ø.5399E-Ø4	Ø.5374E-Ø4
66.Ø	Ø.ØØØØE+ØØ	Ø.1198E-Ø3	Ø.1186E-Ø3
69.Ø	Ø.ØØØØE+ØØ	Ø.1977E-Ø3	Ø.1933E-Ø3

Table X

THETA (DEG)	MAGNITUDE OF VECTOR POTENTIAL		
	TRIANGULAR CURRENT DISTRIBUTION		
	R = 5.Ø	M = 5ØØ	K = 63.
	FAR-FIELD	ICF	NUMERICAL
15.Ø	Ø.ØØØØE+ØØ	Ø.8399E-Ø5	Ø.8398E-Ø5
18.Ø	Ø.ØØØØE+ØØ	Ø.1643E-Ø4	Ø.1643E-Ø4
21.Ø	Ø.ØØØØE+ØØ	Ø.2686E-Ø4	Ø.2684E-Ø4
24.Ø	Ø.ØØØØE+ØØ	Ø.3642E-Ø4	Ø.364ØE-Ø4
27.Ø	Ø.ØØØØE+ØØ	Ø.396ØE-Ø4	Ø.3956E-Ø4
3Ø.Ø	Ø.ØØØØE+ØØ	Ø.3154E-Ø4	Ø.315ØE-Ø4
33.Ø	Ø.ØØØØE+ØØ	Ø.1466E-Ø4	Ø.1464E-Ø4
36.Ø	Ø.ØØØØE+ØØ	Ø.1187E-Ø4	Ø.1187E-Ø4
39.Ø	Ø.ØØØØE+ØØ	Ø.1874E-Ø4	Ø.1872E-Ø4
42.Ø	Ø.ØØØØE+ØØ	Ø.3737E-Ø4	Ø.3734E-Ø4
45.Ø	Ø.ØØØØE+ØØ	Ø.6Ø36E-Ø4	Ø.6Ø3ØE-Ø4
48.Ø	Ø.ØØØØE+ØØ	Ø.4889E-Ø4	Ø.4883E-Ø4
51.Ø	Ø.ØØØØE+ØØ	Ø.2449E-Ø4	Ø.2449E-Ø4
54.Ø	Ø.ØØØØE+ØØ	Ø.5Ø28E-Ø4	Ø.5Ø19E-Ø4
57.Ø	Ø.ØØØØE+ØØ	Ø.746ØE-Ø4	Ø.7441E-Ø4
6Ø.Ø	Ø.ØØØØE+ØØ	Ø.1128E-Ø3	Ø.1124E-Ø3
63.Ø	Ø.ØØØØE+ØØ	Ø.5399E-Ø4	Ø.54ØØE-Ø4
66.Ø	Ø.ØØØØE+ØØ	Ø.1198E-Ø3	Ø.1189E-Ø3
69.Ø	Ø.ØØØØE+ØØ	Ø.1977E-Ø3	Ø.1935E-Ø3

Table XI

THETA (DEG)	MAGNITUDE OF VECTOR POTENTIAL		
	TRIANGULAR CURRENT DISTRIBUTION		
	R = 25.Ø	M = 5Ø	K = 63.
	FAR-FIELD	ICF	NUMERICAL
15.Ø	Ø.155ØE-Ø5	Ø.1555E-Ø5	Ø.1449E-Ø5
18.Ø	Ø.3146E-Ø5	Ø.3152E-Ø5	Ø.2946E-Ø5
21.Ø	Ø.524ØE-Ø5	Ø.5245E-Ø5	Ø.49Ø4E-Ø5
24.Ø	Ø.7213E-Ø5	Ø.7216E-Ø5	Ø.6759E-Ø5
27.Ø	Ø.7995E-Ø5	Ø.7992E-Ø5	Ø.7527E-Ø5
3Ø.Ø	Ø.66Ø8E-Ø5	Ø.6596E-Ø5	Ø.6242E-Ø5
33.Ø	Ø.3277E-Ø5	Ø.3262E-Ø5	Ø.3Ø83E-Ø5
36.Ø	Ø.2993E-Ø6	Ø.5441E-Ø6	Ø.5145E-Ø6
39.Ø	Ø.1Ø92E-Ø5	Ø.13Ø7E-Ø5	Ø.1247E-Ø5
42.Ø	Ø.6693E-Ø5	Ø.6729E-Ø5	Ø.6462E-Ø5
45.Ø	Ø.1258E-Ø4	Ø.1256E-Ø4	Ø.1211E-Ø4
48.Ø	Ø.1154E-Ø4	Ø.1147E-Ø4	Ø.1111E-Ø4
51.Ø	Ø.3548E-Ø5	Ø.3581E-Ø5	Ø.3481E-Ø5
54.Ø	Ø.5141E-Ø6	Ø.2Ø95E-Ø5	Ø.2Ø36E-Ø5
57.Ø	Ø.1214E-Ø4	Ø.1228E-Ø4	Ø.12Ø4E-Ø4
6Ø.Ø	Ø.2565E-Ø4	Ø.2553E-Ø4	Ø.251ØE-Ø4
63.Ø	Ø.181ØE-Ø4	Ø.178ØE-Ø4	Ø.1755E-Ø4
66.Ø	Ø.583ØE-Ø6	Ø.4616E-Ø5	Ø.4572E-Ø5
69.Ø	Ø.1776E-Ø4	Ø.1918E-Ø4	Ø.19Ø1E-Ø4

Table XII

THETA (DEG)	MAGNITUDE OF VECTOR POTENTIAL		
	TRIANGULAR CURRENT DISTRIBUTION		
	R = 25.Ø	M = 1ØØ	K = 63.
	FAR-FIELD	ICF	NUMERICAL
15.Ø	Ø.155ØE-Ø5	Ø.1555E-Ø5	Ø.1524E-Ø5
18.Ø	Ø.3146E-Ø5	Ø.3152E-Ø5	Ø.31ØØE-Ø5
21.Ø	Ø.524ØE-Ø5	Ø.5245E-Ø5	Ø.5168E-Ø5
24.Ø	Ø.7213E-Ø5	Ø.7216E-Ø5	Ø.7113E-Ø5
27.Ø	Ø.7995E-Ø5	Ø.7992E-Ø5	Ø.7878E-Ø5
3Ø.Ø	Ø.66Ø8E-Ø5	Ø.6596E-Ø5	Ø.6518E-Ø5
33.Ø	Ø.3277E-Ø5	Ø.3262E-Ø5	Ø.3228E-Ø5
36.Ø	Ø.2993E-Ø6	Ø.5441E-Ø6	Ø.5385E-Ø6
39.Ø	Ø.1Ø92E-Ø5	Ø.13Ø7E-Ø5	Ø.1297E-Ø5
42.Ø	Ø.6693E-Ø5	Ø.6729E-Ø5	Ø.6672E-Ø5
45.Ø	Ø.1258E-Ø4	Ø.1256E-Ø4	Ø.1245E-Ø4
48.Ø	Ø.1154E-Ø4	Ø.1147E-Ø4	Ø.1138E-Ø4
51.Ø	Ø.3548E-Ø5	Ø.3581E-Ø5	Ø.3552E-Ø5
54.Ø	Ø.5141E-Ø6	Ø.2Ø95E-Ø5	Ø.2Ø82E-Ø5
57.Ø	Ø.1214E-Ø4	Ø.1228E-Ø4	Ø.1222E-Ø4
6Ø.Ø	Ø.2565E-Ø4	Ø.2553E-Ø4	Ø.2543E-Ø4
63.Ø	Ø.181ØE-Ø4	Ø.178ØE-Ø4	Ø.1773E-Ø4
66.Ø	Ø.583ØE-Ø6	Ø.4616E-Ø5	Ø.4599E-Ø5
69.Ø	Ø.1776E-Ø4	Ø.1918E-Ø4	Ø.1912E-Ø4

Table XIII

THETA (DEG)	MAGNITUDE OF VECTOR POTENTIAL		
	TRIANGULAR CURRENT DISTRIBUTION		
	R = 25.Ø	M = 5ØØ	K = 63.
	FAR-FIELD	ICF	NUMERICAL
15.Ø	Ø.155ØE-Ø5	Ø.1555E-Ø5	Ø.1554E-Ø5
18.Ø	Ø.3146E-Ø5	Ø.3152E-Ø5	Ø.3148E-Ø5
21.Ø	Ø.524ØE-Ø5	Ø.5245E-Ø5	Ø.5242E-Ø5
24.Ø	Ø.7213E-Ø5	Ø.7216E-Ø5	Ø.7214E-Ø5
27.Ø	Ø.7995E-Ø5	Ø.7992E-Ø5	Ø.7985E-Ø5
3Ø.Ø	Ø.66Ø8E-Ø5	Ø.6596E-Ø5	Ø.6591E-Ø5
33.Ø	Ø.3277E-Ø5	Ø.3262E-Ø5	Ø.3259E-Ø5
36.Ø	Ø.2993E-Ø6	Ø.5441E-Ø6	Ø.548ØE-Ø6
39.Ø	Ø.1Ø92E-Ø5	Ø.13Ø7E-Ø5	Ø.13Ø6E-Ø5
42.Ø	Ø.6693E-Ø5	Ø.6729E-Ø5	Ø.6728E-Ø5
45.Ø	Ø.1258E-Ø4	Ø.1256E-Ø4	Ø.1256E-Ø4
48.Ø	Ø.1154E-Ø4	Ø.1147E-Ø4	Ø.1147E-Ø4
51.Ø	Ø.3548E-Ø5	Ø.3581E-Ø5	Ø.3581E-Ø5
54.Ø	Ø.5141E-Ø6	Ø.2Ø95E-Ø5	Ø.2Ø93E-Ø5
57.Ø	Ø.1214E-Ø4	Ø.1228E-Ø4	Ø.1228E-Ø4
6Ø.Ø	Ø.2565E-Ø4	Ø.2553E-Ø4	Ø.2553E-Ø4
63.Ø	Ø.181ØE-Ø4	Ø.178ØE-Ø4	Ø.1779E-Ø4
66.Ø	Ø.583ØE-Ø6	Ø.4616E-Ø5	Ø.4617E-Ø5
69.Ø	Ø.1776E-Ø4	Ø.1918E-Ø4	Ø.1916E-Ø4

Table XIV

THETA (DEG)	MAGNITUDE OF VECTOR POTENTIAL		
	TRIANGULAR CURRENT DISTRIBUTION		
	R = 5Ø.Ø	M = 5Ø	K = 63.
	FAR-FIELD	ICF	NUMERICAL
15.Ø	Ø.7748E-Ø6	Ø.7752E-Ø6	Ø.7Ø84E-Ø6
18.Ø	Ø.1573E-Ø5	Ø.1574E-Ø5	Ø.1468E-Ø5
21.Ø	Ø.262ØE-Ø5	Ø.2621E-Ø5	Ø.2448E-Ø5
24.Ø	Ø.36Ø6E-Ø5	Ø.36Ø7E-Ø5	Ø.3395E-Ø5
27.Ø	Ø.3997E-Ø5	Ø.3997E-Ø5	Ø.3767E-Ø5
3Ø.Ø	Ø.33Ø4E-Ø5	Ø.33Ø2E-Ø5	Ø.3112E-Ø5
33.Ø	Ø.1638E-Ø5	Ø.1636E-Ø5	Ø.1555E-Ø5
36.Ø	Ø.1497E-Ø6	Ø.1877E-Ø6	Ø.17ØØE-Ø6
39.Ø	Ø.5458E-Ø6	Ø.5746E-Ø6	Ø.553ØE-Ø6
42.Ø	Ø.3347E-Ø5	Ø.3351E-Ø5	Ø.3213E-Ø5
45.Ø	Ø.6289E-Ø5	Ø.6286E-Ø5	Ø.6Ø7ØE-Ø5
48.Ø	Ø.5771E-Ø5	Ø.5762E-Ø5	Ø.5591E-Ø5
51.Ø	Ø.1774E-Ø5	Ø.1773E-Ø5	Ø.1738E-Ø5
54.Ø	Ø.257ØE-Ø6	Ø.5693E-Ø6	Ø.5579E-Ø6
57.Ø	Ø.6Ø69E-Ø5	Ø.6Ø87E-Ø5	Ø.5953E-Ø5
6Ø.Ø	Ø.1283E-Ø4	Ø.1281E-Ø4	Ø.1259E-Ø4
63.Ø	Ø.9Ø49E-Ø5	Ø.9Ø12E-Ø5	Ø.8885E-Ø5
66.Ø	Ø.2915E-Ø6	Ø.118ØE-Ø5	Ø.1162E-Ø5
69.Ø	Ø.8882E-Ø5	Ø.9Ø64E-Ø5	Ø.8996E-Ø5

Bibliography

1. Meyer-Brendt, Jurgen R. M. D., Introduction to Classical and Modern Optics, Second Edition. Englewood Cliffs, New Jersey: Prentice-Hall, Inc. 1984.

2. Balanis, Constantine A. Antenna Theory Analysis and Design. New York: Harper & Row, Publishers, 1982.

3. Stutzman, Warren L. and Gary A. Thiele. Antenna Theory and Design. New York: John Wiley & Sons, 1981.

4. Tanner, R. L., M. G. Andreason. "Numerical Solution of Electromagnetic Problems," IEEE Spectrum: 54-61 (September 1967).

5. Lee, David A. et al. "Exact Solutions for Radiation from Rectangular and Triangular Current Distributions on Dipoles", To Be Published.

6. Valkenburg, M. E. Van. Network Analysis. Englewood Cliffs, New Jersey: Prentice-Hall, Inc., 1974.

7. Oppenheim, Alan V. and Ronald W. Schafer. Digital Signal Processing. Englewood Cliffs, New Jersey: Prentice-Hall, Inc., 1975.

8. Terzuoli, A. J. Dr. Department of Electrical and Computer Engineering, School of Engineering. W.P.A.F.B., OH., Personal Conversations With.

9. Prescott, G. E. Capt. Department of Electrical and Computer Engineering, School of Engineering. W.P.A.F.B., OH., Personal Conversations With.

10. Ludwig, A. C. "Computation of Radiation Patterns Involving Numerical Double Integration", IEEE Transactions on Antennas and Propagation: 767-769 (November 1968)

11. Miller, E. K. et al. "Numerical Integration Methods", IEEE Transactions on Amtennas and Propagation: 669-672 (September 1969).

12. Richmond, J. H. "The Numerical Evaluation of Radiation Integrals", IRE Transactions on Antennas and Propagation, 358-360 (1961).

13. Allen, Charles C. "Numerical Integration Methods for Antenna Pattern Calculations", IRE Transactions on Antennas and Propagation, AP-7 SP. Supp: S387-S401 (December 1959).

14. Burden, Richard L., J. Douglas Faires, Albert C. Reynolds, Numerical Analysis Second Edition. Boston, Mass: Prindle, Weber & Schmidt, 1981.

15. Pyati, V. P. Dr. Department of Electrical and Computer Engineering, School of Engineering. W.P.A.F.B., OH., Personal Conversations With.

16. Filon, Proc. Roy. Soc. Edinburgh, (A) 49:38 (1928)

17. Kopal, Zdenek, Numerical Analysis. London: Chapman & Hall Ltd, 1961.

18. Davis, Philip J. and Philip Rabinowitz. Numerical Integration. Waltham, Mass.: Blaisdell Publishing Co., 1967.

19. Lee, David A. Head of Department of Mathematics & Computer Science, School of Engineering, Air Force Institute of Technology. W.P.A.F.B., OH., Personal Conversations With.

20. Jones, J. Jr. Dr. Department of Mathematics & Computer Science, School of Engineering, Air Force Institute of Technology. W.P.A.F.B., OH., Personal Conversations With.

21. Clemens, G. P. Capt., Department of Mathematics & Computer Science, School of Engineering, Air Force Institute of Technology. W.P.A.F.B., OH., Personal Conversations With.

22. Agrest, M. M. and M. S. Maksimov. Theory of Incomplete Cylindrical Functions and Their Applications. Berlin, Germany: Springer-Verlag (1971).

23. Linderman, R. W. Capt., Department of Electrical and Computer Engineering, School of Engineering, Air Force Institute of Technology. W.P.A.F.B., OH., Personal Conversations With.

24. Ware, Fredrick A. "A 64b Floating Point Processor", IEEE International Solid-State Circuits Conference: 24 (February 1982).

25. Anderson, S. F. et al. "The IBM System/360 Model 91 Floating Point Execution Unit", IBM Journal of Research and Development, 11: 48-52 (1967).

26. Zurawski, J. H. P. and J. B. Gosling. "Design of High-Speed Digital Divider Units", IEEE Transactions on Computers, C-30, No. 9: (September 1981).

27. Bridge, Carol L. et al. "Asynchronous Arithmetic Algorithm for Data Driven Machines", Proceedings of the Fifth IEEE Symposium on Computer Arithmethic: 59 (May 1981).

28. Banerji, Dilip K. and Saroj Kaushik. "Representation and Processing of Fractions in a Residue System", Proc. 6TH IEEE Symposium on Computer Arithmetic: 34-35 (June 1983).

29. Taylor, George S. "Radix 16 SRT Dividers with Overlapped Quotient Selection Stages", Proceedings of the 7TH IEEE Symposium on Computer Arithmetic: 64-71 (June 1985).

30. Ercegovac, M. D. and T. Lang. "A Division Algorithm with Prediction of Quotient Digits", Proceedings of the 7TH IEEE Symposium on Computer Arithmetic: 51-56 (June 1985).

31. Cavanagh, Joseph J. F. Digital Computer Arithetic: Design and Implementation. New York: McGraw Hill Inc., 1984.

32. Abramowitz, Milton and Irene A. Stegun. Handbook of Mathematical Functions with Formulas, Graphs, and Mathematical Tables. United States Department of Commerce, National Bureau of Standards, Applied Mathematics Series: 55, 1964.

33. Quinn, D. W. Dr. Department of Mathematics and Computer Science, School of Engineering, Air Force Institute of Technology. W.P.A.F.B., OH. Personal Conversations With.

34. Volder, Jack E. "The Cordic Trigonometric Computing Technique", IRE Transactions on Electronic Computers: 330-334 (September 1959).

35. Steer, D. G. and S. R. Penstone. "Digital Hardware for Sine-Cosine Function", IEEE Transactions on Computers, C-26, No. 12: 1283-1286.

36. Naseem, Asif and P. David Fisher. "The Modified Cordic Algorithm", Proceedings of the 7TH IEEE Symposium on Computer Arithmetic: 144-152 (June 1985).

37. Thomas, George B. Jr. Calculus and Analytic Geometry. Reading, Mass.: Addison-Wesley Publishing Co. Inc. 1972.

38. Chen, Tien Chi. "Automatic Computation of Exponentials, Logarithms, Ratios and Square Roots", IBM Journal of Research and Development, 16: 380-388 (July 1972).

39. Banner, J. and A. Varma. "The VLSI Implementation of a Square Root Algorithm", Proceedings of the 7TH IEEE Symposium on Computer Arithmetic: 159-165 (June 1985).

VITA

Captain Lawrence E. Jones was born on 22 July 1947 in Cheyenne, Wyoming. He graduated from high school in 1965, and attended the University of Wyoming for one year before entering the USAF. As an enlisted member he performed duties in career fields, 32550 (Automatic Pilot System Specialist) and 32470 (Precision Measurement Equipment Technician). He was accepted into the Airman Education and Commissioning program in January 1979, and ultimately graduated from Texas A & M University in May 1981, BSEE Cum Laude. After completing OTS August 1981, (DG), he was assigned to the 6585 TG Holloman AFB, New Mexico. There he performed as an electrical and computer system design engineer, where he designed and fabricated digital and analog hardware for use in interfacing guidance systems to an HP 1000 computer. He was awarded the Air Force Commendation Medal upon leaving Holloman and entering the school of Engineering, at the Air Force Institute of Technology WPAFB,OH in May 1984.

Permanent address: 2017 Dunn
Cheyenne, Wyoming
82001

UNCLASSIFIED

SECURITY CLASSIFICATION OF THIS PAGE

AD-A163 925

REPORT DOCUMENTATION PAGE

1a. REPORT SECURITY CLASSIFICATION: UNCLASSIFIED

1b. RESTRICTIVE MARKINGS:

2a. SECURITY CLASSIFICATION AUTHORITY:

2b. DECLASSIFICATION/DOWNGRADING SCHEDULE:

3. DISTRIBUTION/AVAILABILITY OF REPORT: Approved for public release; distribution unlimited.

4. PERFORMING ORGANIZATION REPORT NUMBER(S): AFIT/GE/ENG/85D-23

5. MONITORING ORGANIZATION REPORT NUMBER(S):

6a. NAME OF PERFORMING ORGANIZATION: School of Engineering

6b. OFFICE SYMBOL (If applicable): AFIT/ENG

7a. NAME OF MONITORING ORGANIZATION:

6c. ADDRESS (City, State and ZIP Code): Air Force Institute of Technology, Wright-Patterson AFB, Ohio 45433

7b. ADDRESS (City, State and ZIP Code):

8a. NAME OF FUNDING/SPONSORING ORGANIZATION:

8b. OFFICE SYMBOL (If applicable):

9. PROCUREMENT INSTRUMENT IDENTIFICATION NUMBER:

8c. ADDRESS (City, State and ZIP Code):

10. SOURCE OF FUNDING NOS.

PROGRAM ELEMENT NO.	PROJECT NO.	TASK NO.	WORK UNIT NO.

11. TITLE (Include Security Classification): See Box 19

12. PERSONAL AUTHOR(S): Lawrence E. Jones, B.S., Captain, USAF

13a. TYPE OF REPORT: MS Thesis

13b. TIME COVERED: FROM ________ TO ________

14. DATE OF REPORT (Yr., Mo., Day): 1985 December

15. PAGE COUNT:

16. SUPPLEMENTARY NOTATION:

17. COSATI CODES

FIELD	GROUP	SUB. GR.
09	01	

18. SUBJECT TERMS (Continue on reverse if necessary and identify by block number): Radiation Integral, Three-Dimensional, Digital Algorithm

19. ABSTRACT (Continue on reverse if necessary and identify by block number)

Title: ALGORITHM DEFINITION FOR THE VLSI DESIGN IMPLEMENTATION OF THE ELECTROMAGNETIC RADIATION INTEGRAL

Thesis Chairman: Dr. A. J. Terzuoli

Approved for public release: IAW AFR 190-1.
Lynn E. Wolaver 16 JAN 86
LYNN E. WOLAVER
Dean for Research and Professional Development
Air Force Institute of Technology (AFC)
Wright-Patterson AFB OH 45433

20. DISTRIBUTION/AVAILABILITY OF ABSTRACT: UNCLASSIFIED/UNLIMITED ☒ SAME AS RPT ☐ DTIC USERS ☐

21. ABSTRACT SECURITY CLASSIFICATION: UNCLASSIFIED

22a. NAME OF RESPONSIBLE INDIVIDUAL: Dr. A. J. Terzuoli

22b. TELEPHONE NUMBER (Include Area Code): 513-255-6913

22c. OFFICE SYMBOL: AFIT/ENG

DD FORM 1473, 83 APR EDITION OF 1 JAN 73 IS OBSOLETE.

UNCLASSIFIED

SECURITY CLASSIFICATION OF THIS PAGE

A classic method used to solve for the electric (E) and magnetic (H) fields produced by a radiating source involves first solving for the vector potential (A) through the evaluation of the radiation integral. This study was undertaken to define a numerical algorithm that solves for A, so that a reduction in computation time can be realized through VLSI design implementation.

Fast Fourier Transforms, Newton-Cotes numerical integration, and variable parameterization, were applied to the problem with unsuccessful results. A numerical summation approximation proved to have all the desired qualities for the algorithm. These qualities are, ability to handle arbitrary antennas, accurate results, and all digital mathematics algorithms exist. Verification of the numerical solution was accomplished by comparing the results it produced for a dipole antenna with a triangular shaped current density against the far-field approximation, and an incomplete cylindrical functions solution developed by Lee.

Solution for E and H involves taking derivatives of A. Complications that arise from numerical techniques dictate that numerical differentiation should be performed before numerical integration. Follow on work on this topic will therefore have to focus on this detail before the actual VLSI chip architecture definition stage can be addressed.